

AWARD NUMBER: W81XWH-13-1-0202

TITLE: Functional Genomics to Identify Therapeutic Targets in Cancer Stem Cells Using a Novel Murine CRPC Model

PRINCIPAL INVESTIGATOR: Dr. Guocan Wang

CONTRACTING ORGANIZATION: The University of Texas MD Anderson Cancer Center
Houston, TX 77030

REPORT DATE: November 2015

TYPE OF REPORT: Final Report

PREPARED FOR: U.S. Army Medical Research and Materiel Command
Fort Detrick, Maryland 21702-5012

DISTRIBUTION STATEMENT: Approved for public release; distribution is unlimited.

The views, opinions and/or findings contained in this report are those of the author(s) and should not be construed as an official Department of the Army position, policy or decision unless so designated by other documentation.

REPORT DOCUMENTATION PAGE				Form Approved OMB No. 0704-0188	
Public reporting burden for this collection of information is estimated to average 1 hour per response, including the time for reviewing instructions, searching existing data sources, gathering and maintaining the data needed, and completing and reviewing this collection of information. Send comments regarding this burden estimate or any other aspect of this collection of information, including suggestions for reducing this burden to Department of Defense, Washington Headquarters Services, Directorate for Information Operations and Reports (0704-0188), 1215 Jefferson Davis Highway, Suite 1204, Arlington, VA 22202-4302. Respondents should be aware that notwithstanding any other provision of law, no person shall be subject to any penalty for failing to comply with a collection of information if it does not display a currently valid OMB control number. PLEASE DO NOT RETURN YOUR FORM TO THE ABOVE ADDRESS.					
1. REPORT DATE November 2015		2. REPORT TYPE FINAL REPORT		3. DATES COVERED 6 Aug 2013 - 5 Aug 2015	
4. TITLE AND SUBTITLE Functional Genomics to Identify Therapeutic Targets in Cancer Stem Cells Using a Novel Murine CRPC Model				5a. CONTRACT NUMBER	
				5b. GRANT NUMBER W81XWH-13-1-0202	
				5c. PROGRAM ELEMENT NUMBER	
6. AUTHOR(S) Dr. Guocan Wang E-Mail: GWang6@mdanderson.org				5d. PROJECT NUMBER	
				5e. TASK NUMBER	
				5f. WORK UNIT NUMBER	
7. PERFORMING ORGANIZATION NAME(S) AND ADDRESS(ES) The University of Texas MD Anderson Cancer Center 1515 Holcombe Boulevard Houston, TX 77030-4009				8. PERFORMING ORGANIZATION REPORT NUMBER	
9. SPONSORING / MONITORING AGENCY NAME(S) AND ADDRESS(ES) U.S. Army Medical Research and Materiel Command Fort Detrick, Maryland 21702-5012				10. SPONSOR/MONITOR'S ACRONYM(S)	
				11. SPONSOR/MONITOR'S REPORT NUMBER(S)	
12. DISTRIBUTION / AVAILABILITY STATEMENT Approved for Public Release; Distribution Unlimited					
13. SUPPLEMENTARY NOTES					
14. ABSTRACT Castration resistant prostate cancer (CRPC) still remains as a major clinical challenge, since they are incurable. Prostate stem cells can be the cell of origin for prostate cancers accounting for the development of CRPC. However, the identity of prostate cancer stem cells in CRPC remains elusive. Here I used a metastatic <i>Pten^{pc/-}Smad4^{pc/-}</i> mouse prostate cancer model to study the mechanisms for CRPC and the biology of cancer stem cells. I discovered that <i>Pten^{pc/-}Smad4^{pc/-}</i> tumors have de novo resistance to ADT as compared to <i>Pten^{pc/-}</i> tumors, although castration did provide some survival benefits for <i>Pten^{pc/-}Smad4^{pc/-}</i> mice. Established <i>Pten^{pc/-}Smad4^{pc/-}</i> CRPC tumors show an increase in proliferating basal cells, the putative cancer stem cells population in castrated <i>Pten^{pc/-}Smad4^{pc/-}</i> prostate tumors. ADT in <i>Pten^{pc/-}Smad4^{pc/-}</i> mice may promote massive lung metastasis. Interestingly, by integrative analysis of transcriptomic data I identified pathways that may play a role in the resistance to ADT and cancer stem cells in the <i>Pten^{pc/-}Smad4^{pc/-}</i> tumors, such as Hippo/Yap1, and Sox2. Importantly, we identify tumor-intrinsic mechanisms as well as tumor-extrinsic mechanisms which not only promote tumor progression but also castration resistance. Particularly, we identified myeloid-derived suppressor cells (MDSCs) as a key regulator in these processes, which is mediated by the activation of Yap1-Cxcl5-Cxcr2 axis.					
15. SUBJECT TERMS Prostate cancer, Genetically engineered mouse model, Castration resistance prostate cancer, cancer stem cell, tumor microenvironment, Yap1, Myeloid-derived suppressor cells (MDSCs), Cxcl5, Cxcr2.					
16. SECURITY CLASSIFICATION OF: U			17. LIMITATION OF ABSTRACT Unclassified	18. NUMBER OF PAGES 42	19a. NAME OF RESPONSIBLE PERSON USAMRMC
a. REPORT Unclassified	b. ABSTRACT Unclassified	c. THIS PAGE Unclassified			19b. TELEPHONE NUMBER (include area code)

Table of Contents

	<u>Page</u>
1. Introduction.....	4
2. Keywords.....	4
3. Accomplishments.....	4
4. Impact.....	21
5. Changes/Problems.....	21
6. Products.....	21
7. Participants & Other Collaborating Organizations.....	22
8. Special Reporting Requirements.....	23
9. Appendices.....	23

1. INTRODUCTION: Prostate cancer is the most common noncutaneous malignancy in men in the United States[1]. Even though androgen deprivation therapy (ADT), the mainstay of systemic therapy for prostate cancer, has an initial success rate of almost 90%[2], prostate cancer invariably becomes refractory to castration, resulting in the development of lethal castration resistant prostate cancer (CRPC). Although several novel therapies, such as CYP17 inhibitor Abiraterone[3] and the next generation AR inhibitor MDV3100[4], significantly prolong the survival of CRPC patients, there remains a critical need for a better understanding the molecular mechanisms for the development of CRPC. Despite the debatable nature of the prostate stem cells, it is generally believed that prostate stem cells can be the cell of origin for prostate cancers accounting for the development of CRPC. However, the identity of prostate cancer stem cells in CRPC remains elusive, in part due to the lack of amenable animal models with defining properties of human CRPC, including castration-resistance and lethal metastasis. Our pilot study in our metastatic *Pten^{pc/-}Smad4^{pc/-}* mouse model demonstrated a significant tumor growth delay and better survival in the castrated cohort as compared with the control, which recapitulates the temporary benefits of ADT for human prostate cancer patients. However, the castrated mice eventually developed CRPC with metastatic spread to lymph nodes and distant organs (data not shown). Furthermore, BrdU labeling shows an increased in proliferating cells in castrated *Pten^{pc/-}Smad4^{pc/-}* prostate tumors as compared to *Pten^{pc/-}*. Interestingly, it has been demonstrated that Smad4 interacts with AR and regulates AR signaling[5], suggesting a potential role for Smad4 in the development of CRPC. Thus our metastatic prostate cancer model will allow us to generate a humanized CRPC mouse model which will facilitate the process of identifying novel therapeutic targets for CRPC using a functional genomics approach.

2. KEYWORDS: Prostate cancer, Genetically engineered mouse model, Castration resistance prostate cancer, cancer stem cell, tumor microenvironment, Yap1, Myeloid-derived suppressor cells (MDSCs), Cxcl5, Cxcr2.

3. ACCOMPLISHMENTS:

3A. What were the major goals of the project?

Aim 1. Biological characterization of CRPC and tumor-repopulating cells.

Aim 2. Genomic and transcriptomic analysis of CRPC and cancer stem cells.

Aim 3. Functional validation of CRPC genes in cancer stem cells.

3B. What was accomplished under these goals? (1) major activities; 2) specific objectives; 3) significant results or key outcomes, including major findings, developments, or conclusions (both positive and negative); and/or 4) other achievements. Include a discussion of stated goals not met. Description shall include pertinent data and graphs in sufficient detail to explain any significant results achieved. A succinct description of the methodology used shall be provided. As the project progresses to completion, the emphasis in reporting in this section should shift from reporting activities to reporting accomplishments.

Aim 1. Biological characterization of CRPC and tumor-repopulating cells.

Current objects: (a) To characterize the response of *Pten^{pc/-}Smad4^{pc/-}* mutant mice to ADT. We have performed castration in a larger cohort of mice and generated cumulative survival curve for this cohort (Fig.1). We have also collected prostate tissues and non-prostate tissue

from major organs such as bone, lung, and lymph nodes from these mice. In addition, lung and

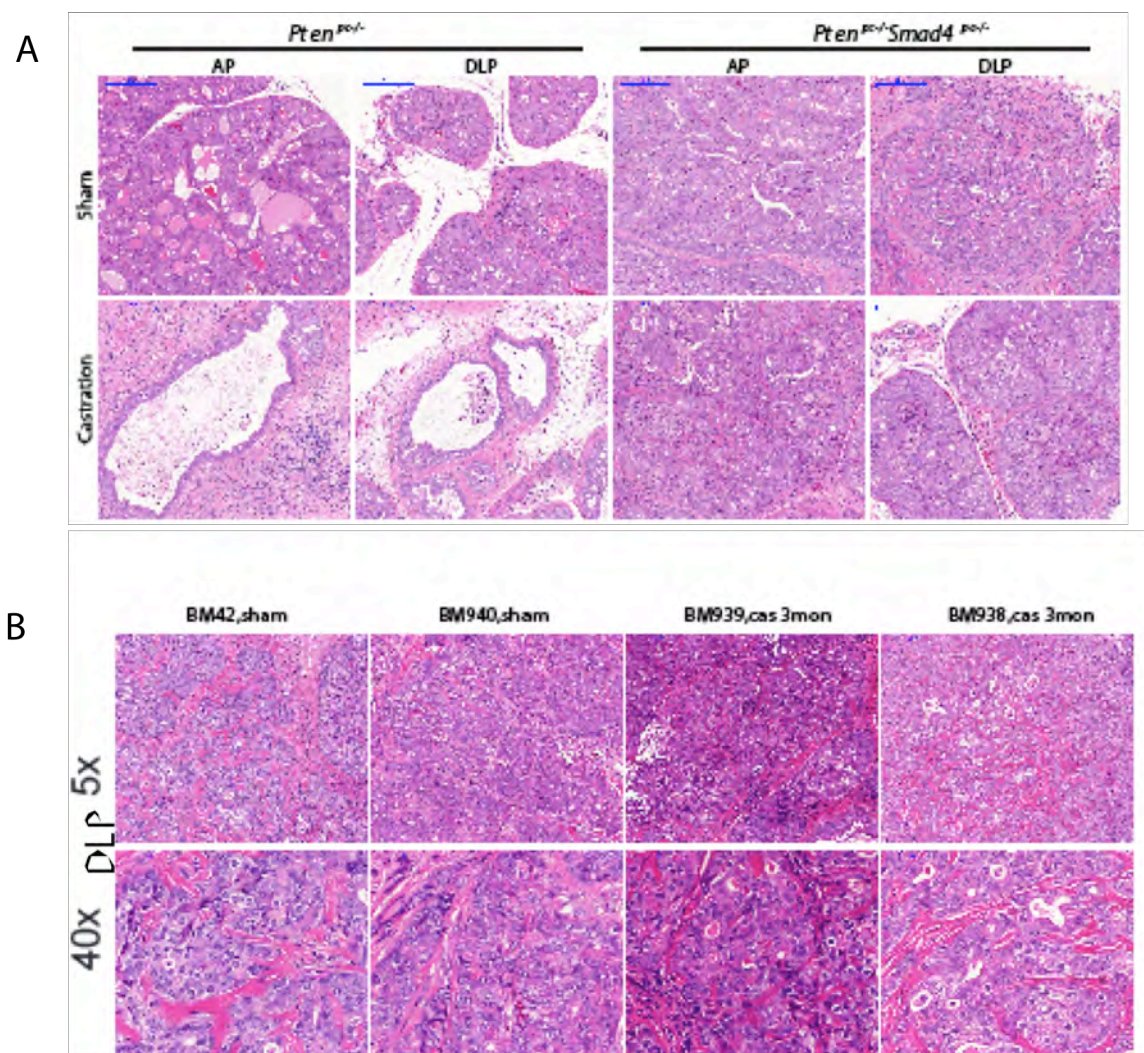


Fig 1. H & E staining of tumors from sham control and castrated mice (*Pten*^{pc/-} *Smad4*^{pc/-} and *Pten*^{pc/-} mice) at 1 month (A) and 3 months (B) post-ADT

bone tissues from *Pten*^{pc/-} *Smad4*^{pc/-} mutant mice with lethal CRPC will be examined for increased lung metastasis and bone metastasis. (b) To characterize cancer stem cells in the treatment naïve prostate tumors and CRPC tumors.

Methodology: Wild type, *Pten*^{pc/-}, and *Pten*^{pc/-} *Smad4*^{pc/-} mice are subjected to surgical castration or in combination with MDV3100 treatment (10 mg/kg daily oral gavage). 5 mice will be sacrificed at 2, 4, 8, and 12 weeks post ADT and tumors and other tissues, such as lung, bones, and lymph nodes, are harvested for histopathological analysis, RNA isolation, Chromatin immunoprecipitation, Western blot analysis, and cancer stem cell sphere assay.

Results:

1. *Pten^{pc/-}Smad4^{pc/-}* tumors are resistant to surgical castration as well as surgical castration plus MDV3100 (also called Enzalutamide). I performed surgical castration alone or in combination with MDV3100 treatment in *Pten^{pc/-}Smad4^{pc/-}* and *Pten^{pc/-}* mice. Tumors were harvested at 2, 4, 8, and 12 weeks post-ADT and subjected to histopathological analysis. In consistent with previous report [6, 7], *Pten^{pc/-}* tumors are sensitive to ADT (Fig 1A). A significant amount of normal epithelium was identified in castrated *Pten^{pc/-}* mice at 1 and 2

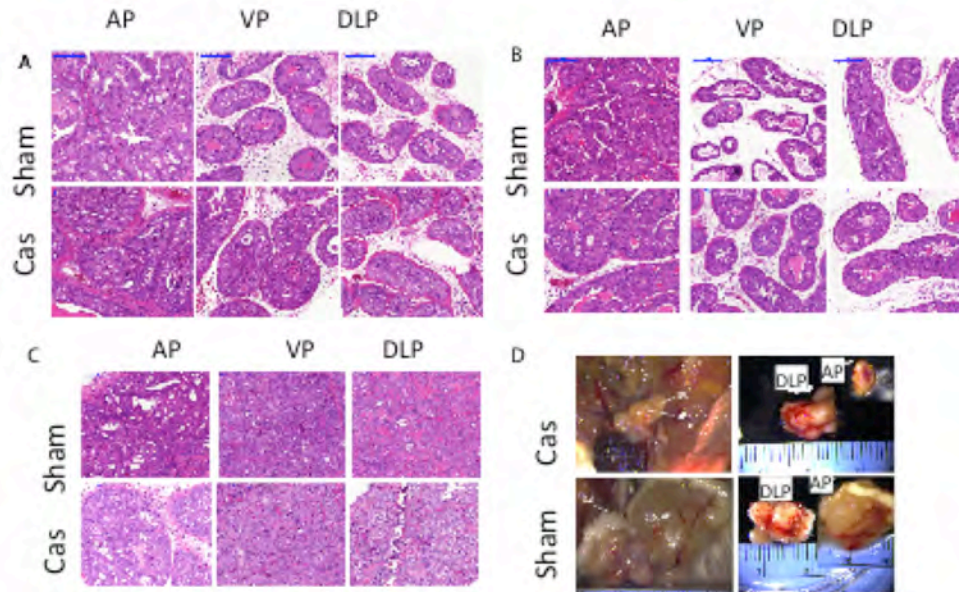


Fig 2. *Pten^{pc/-}Smad4^{pc/-}* tumors are resistance to MDV3100. (A) 2 weeks, (B) 4 weeks, and (C-D) 12 weeks post-castration+MDV3100 treatment.

post-castration[6, 7]. On the contrary, *Pten^{pc/-}Smad4^{pc/-}* mice are resistant to castration as compared to *Pten^{pc/-}* as shown by histopathological analysis by H & E staining (Fig 1A) and MRI analysis (data not shown). There is no noticeable normal epithelium in the castrated *Pten^{pc/-}Smad4^{pc/-}* mice 1, 2, and 3 months post-castration (Fig 1), suggesting loss of *Smad4* in

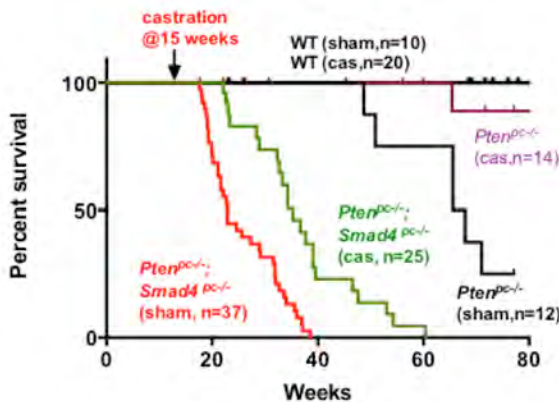


Fig 3. Kaplan Meier survival analysis.

development of CRPC as well as resistance to MDV3100.

months post-castration, suggesting a clear response to castration. Interestingly, the stroma in the castrated *Pten^{pc/-}* mice is significantly expanded, which may account for the emergence of CRPC in *Pten^{pc/-}* mice 3 months

in a *Pten*-null genetic context confers a de novo resistance to ADT. Furthermore, *Pten^{pc/-}Smad4^{pc/-}* prostate tumors are also resistant to a comprehensive AR blockade using surgical castration plus treatment with Enzalutamide, a potent AR inhibitor used in clinic for metastatic CRPC, as shown by H & E staining (Fig 2) and MRI analysis (data not shown). Although ADT did slightly prolong the survival of *Pten^{pc/-}Smad4^{pc/-}* mice, they eventually succumbed to lethal CRPC (Fig 3), suggesting that this unique model may allow the identification of novel pathways that may play a role in the

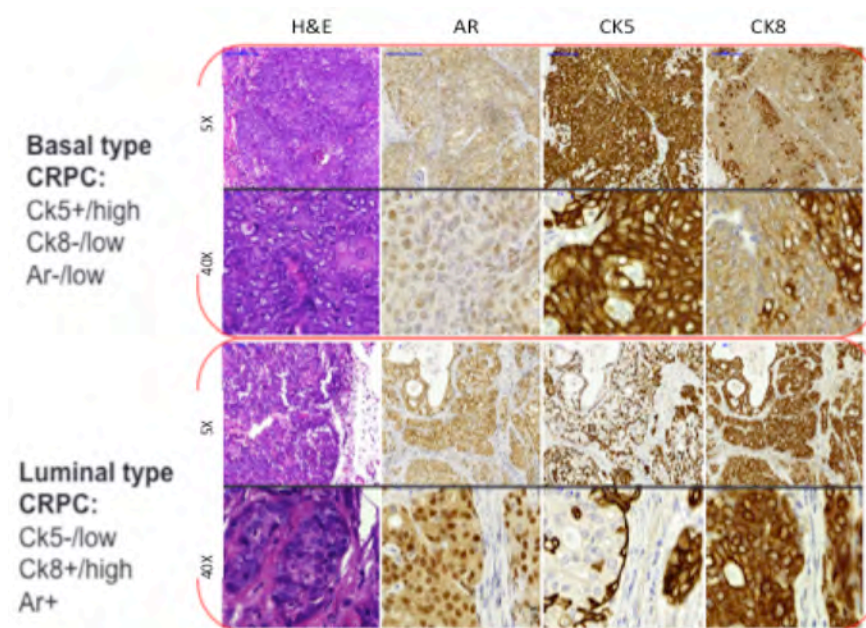


Fig 4. *Pten*^{pc/-}*Smad4*^{pc/-} CRPC tumors display basal and luminal phenotype.

2. *Pten*^{pc/-}*Smad4*^{pc/-} CRPCs display both luminal and basal phenotypes. To fully characterize the lethal CRPC developed at ~3 months post castration, I performed H & E staining and immunohistochemical staining using various verified antibodies for prostatic epithelial origin, such as luminal cell markers (CK8, CK18, Nkx3.1, and AR), and basal cell markers (CK14, CK5, p63). In addition, I also

performed cyclin D1 and Ki67 staining to assess the proliferation of these CRPCs.

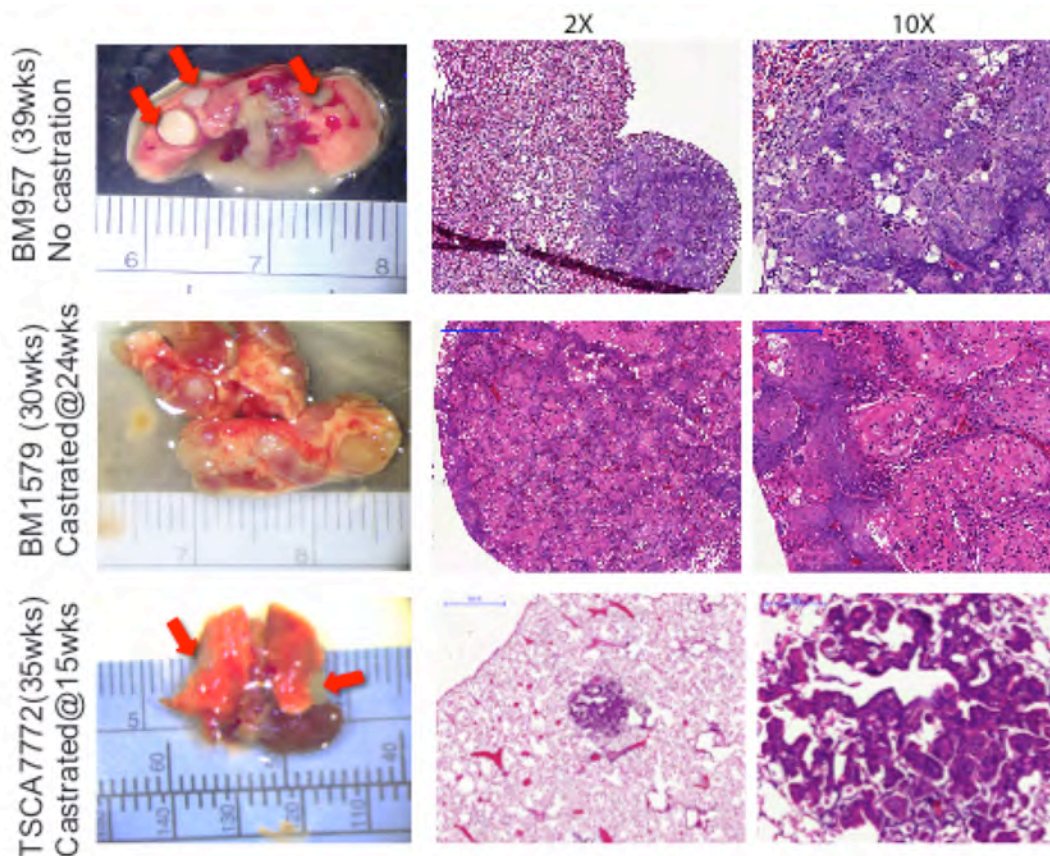


Fig 5. ADT promote massive lung metastasis.

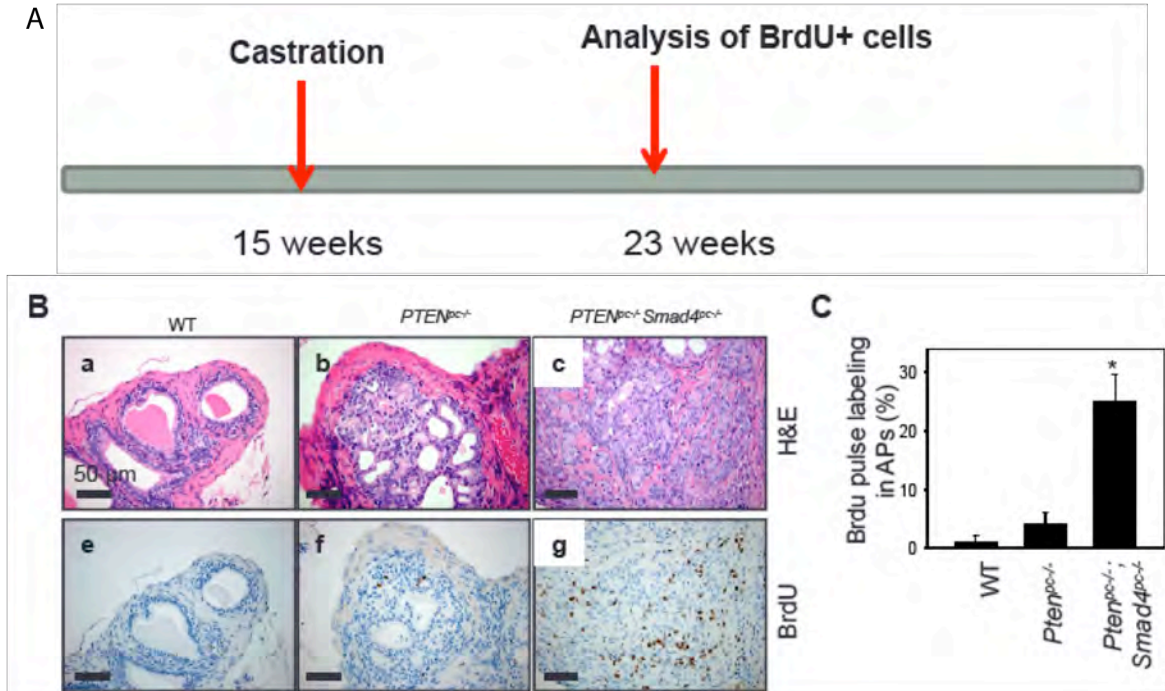


Fig 6. BrdU incorporation experiment in castrated mice. (A) IHC staining for BrdU and (B)

Interestingly, IHC staining shows these CRPCs from *Pten*^{pc/-} *Smad4*^{pc/-} mice display both luminal and basal phenotypes, which are CK18⁺/AR⁺CK5^{low} and CK18^{low}/AR^{low} CK5^{hi} respectively (Fig 4). Consistent with human CRPCs, Ar is reactivated in *Pten*^{pc/-} *Smad4*^{pc/-} tumors as shown by the nuclear staining of Ar (Fig 4). Interestingly, in the treatment naïve prostate *Pten*^{pc/-} *Smad4*^{pc/-} tumors, Ar is expressed in the majority of the cells (data not shown). However, some AR+ tumor cells also expressed strong basal cell markers Ck5 (data not shown), suggesting that such basal type AR+ cells downregulate Ar expression in the CRPC tumors.

3. ADT may promote tumor progression a subset of aggressive *Pten*^{pc/-} *Smad4*^{pc/-} tumors. Given the *Pten*^{pc/-} *Smad4*^{pc/-} mice developed lung metastasis, I examined all control and castrated *Pten*^{pc/-} *Smad4*^{pc/-} mice for lung metastasis. Interestingly, a subset of *Pten*^{pc/-} *Smad4*^{pc/-} mice (n=2) developed massive metastasis in the lung (Fig 5. Middle panel), which is not observed in control mice (Fig 5, top panel), suggesting that although ADT provide some survival benefits for the *Pten*^{pc/-} *Smad4*^{pc/-} mice, it can possibly promote dissemination or the growth of the metastatic tumor cells.

4. Castrated *Pten*^{pc/-}*Smad4*^{pc/-} tumors display increased proliferation as compared to *Pten*^{pc/-} tumors. To assess the proliferative potential of the prostate tumor cells undergone ADT, I performed BrdU incorporation assay. Briefly, BrdU was injected into mice at the age of 15 weeks (wild type, *Pten*^{pc/-}, and *Pten*^{pc/-}*Smad4*^{pc/-} mice) and BrdU incorporation was determined by IHC using a BrdU specific antibody. As shown in Fig 6, castrated *Pten*^{pc/-}*Smad4*^{pc/-} tumors contained significantly more BrdU positive cells than the castrated *Pten*^{pc/-} tumors, which is in line with the de novo resistance to ADT observed in the *Pten*^{pc/-}*Smad4*^{pc/-} tumors. Furthermore, Ki67 staining of the primary tumor and the lung metastasis from the castrated *Pten*^{pc/-}*Smad4*^{pc/-} mice shows that *Pten*^{pc/-}*Smad4*^{pc/-} CRPCs are highly proliferative (Fig 7). In addition, p63+ cells are significantly increased in the castrated *Pten*^{pc/-}*Smad4*^{pc/-} mice (Fig7), suggesting the basal cells contribute significantly to the aggressiveness of the *Pten*^{pc/-}*Smad4*^{pc/-} CRPCs.

5. Cyclin D1 positive cells are mainly CK5+ cells. Since Cyclin D1 has been shown to be overexpressed in the treatment naïve *Pten*^{pc/-}*Smad4*^{pc/-} tumors (ref, Ding 2011), I performed IHC for cyclin D1, Ar, and CK5, in the *Pten*^{pc/-}*Smad4*^{pc/-} CRPCs. Interestingly, Cyclin D1 is

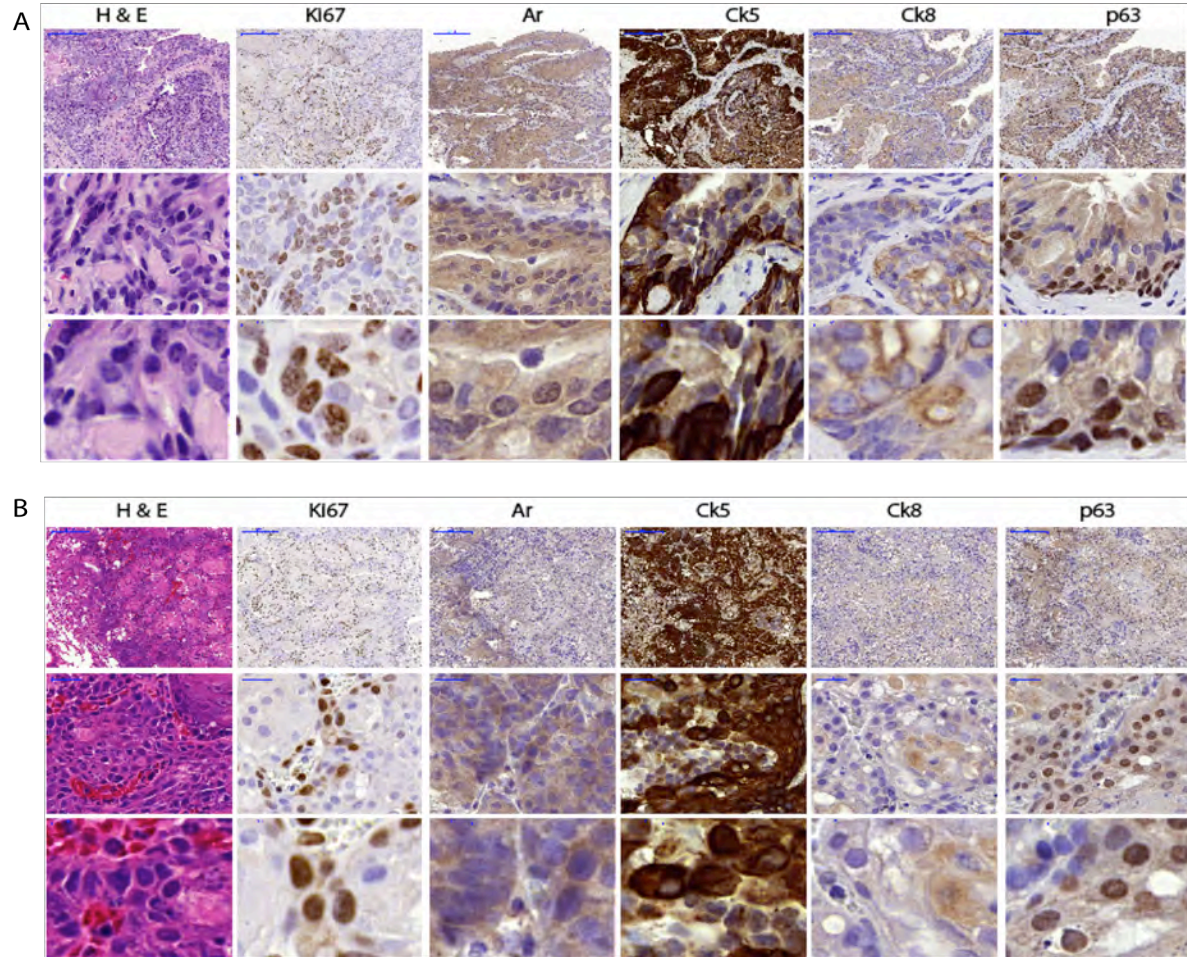


Fig 7. H & E staining and Ki67, Ar, Ck5, Ck9, p63 IHC CRPC primary tumors (A) and lung metastasis (B)

highly expressed in the *Pten*^{pc/-}*Smad4*^{pc/-} CRPCs, which also display high CK5 expression and low Ar expression, suggesting that the majority of the cyclin D1+ cells in the *Pten*^{pc/-}

Smad4^{pc/-} CRPCs are of basal cell properties, which also renders them less dependent on Ar signaling and thus are resistant to ADT.

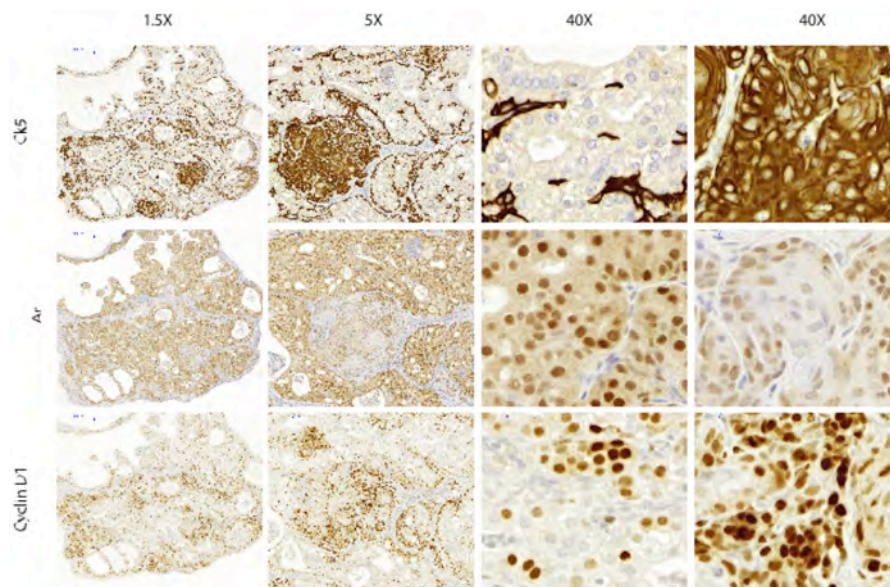


Fig. 8. Cyclin D1 positive cells are mainly CK5+ cells.

Progress, accomplishment and discussion:

I have generated a larger experimental cohort and have completed the Kaplan Meier Survival analysis. The mouse prostate tumors have been subjected to extensive histopathological analysis. I will further characterize the cancer stem cells in the treatment

naïve and castration resistant prostate tumors from *Pten*^{pc/-}*Smad4*^{pc/-} mice.

Aim 2. Genomic and transcriptomic analysis of CRPC and cancer stem cells.

Current objects: The goal of this aim is to utilize powerful genomic profiling technologies to identify novel genes and pathways that drive the development of CRPC. **Methodology:** To

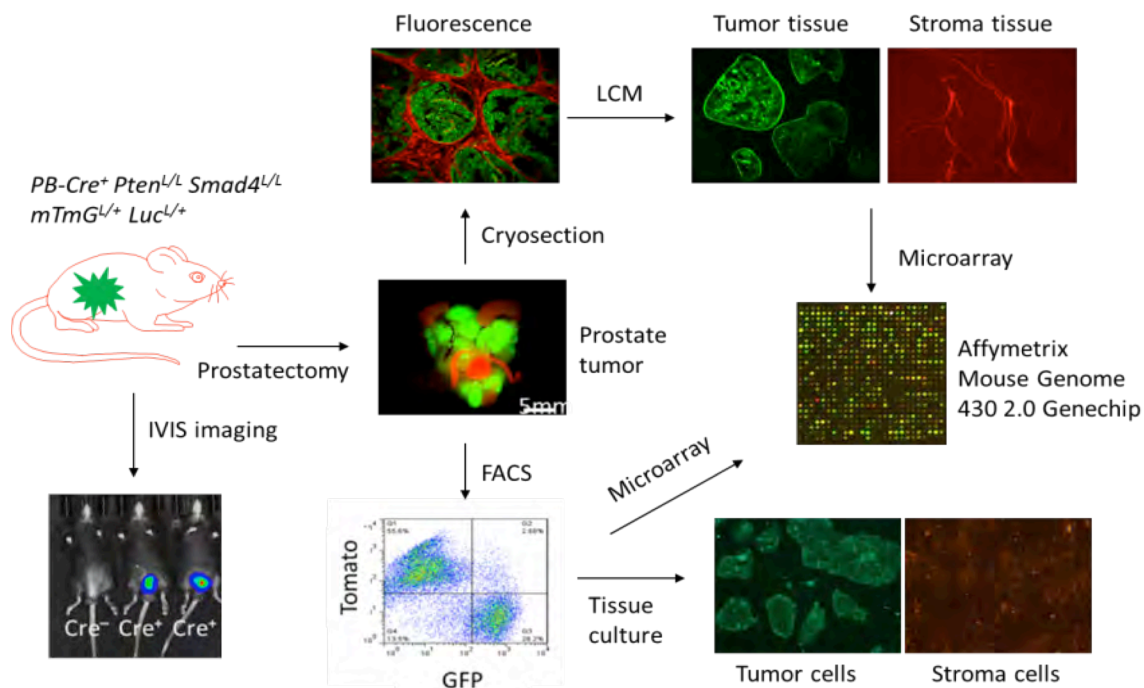


Figure 9. A novel metastatic prostate GEMM with fluorescence and luciferase reporters for noninvasive tracking of tumor growth as well as phenotypic and molecular dissection of tumor and stroma.

enable unambiguous distinction between tumor and stroma, we incorporated a dual fluorescent reporter allele, Rosa26-Lox-tdTomato-Lox-EGFP (a.k.a. mTmG)26, into the PB-Cre+ Pten^{L/L} Smad4^{L/L} model. This allele allows Cre-dependent GFP expression in prostate epithelial cells as well as ubiquitous tdTomato expression in all other cells (Figure 9). We now can (1) visualize tumor and stroma distinctly by fluorescence imaging, (2) visually quantify metastases in lymph node and lung without laborious histological inspection, and (3) easily

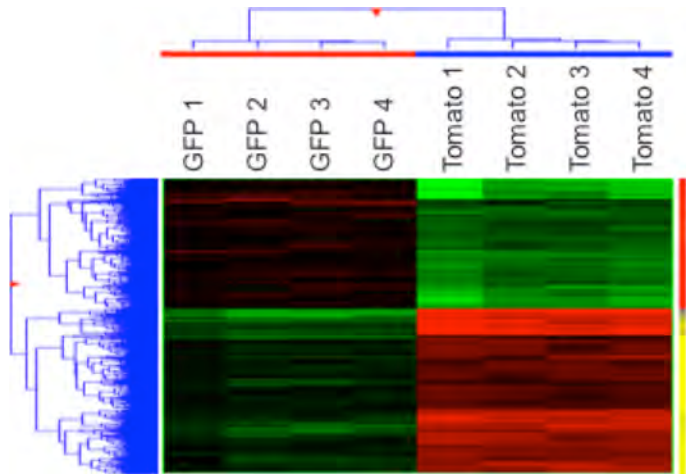


Fig 10. Hierarchical Clustering Analysis of GFP+ tumor cells and Tomato+ stromal cells.

isolate tumor and stromal cells using flow cytometry or Laser Capture Microdissection. Furthermore, to enable noninvasive bioluminescence imaging (BLI) of tumor and metastasis development, we have further incorporated Rosa26-Lox-STOP-Lox-Luciferase allele and have confirmed the prostate-specific luciferase signal (Figure 9). Thus, we now have established a robust metastatic PCa model: PB-Cre⁺ Pten^{L/L} Smad4^{L/L} mTmG^{L/+} Luc^{L/+}, which will facilitate monitoring of tumor development and tumor-stroma interactions through dual fluorescence and bioluminescence imaging. In parallel, we have also established a comparable model with only Pten loss: PB-Cre⁺ Pten^{L/L} mTmG^{L/+} Luc^{L/+}. It is important to note that we have now backcrossed these strains to C57BL/6 congenic background, which enables syngeneic transplantation.

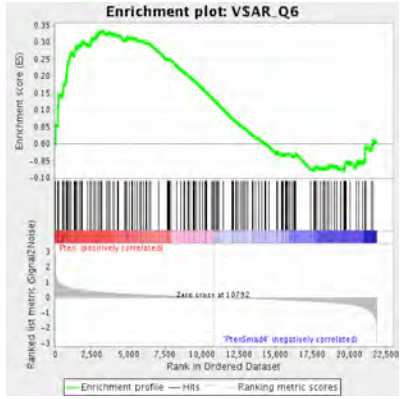
A

1	VSAR_Q6
2	GTGTGAG.MIR-342
3	V\$HNF1_C
4	AAGTCCA.MIR-422B.MIR-422A
5	AAAGGAT.MIR-501
6	GCTCTTG.MIR-335
7	V\$HNF1_Q6
8	GCTGAGT.MIR-512-5P
9	TCANNTGAY_V\$SREBP1_Q1
10	V\$HNF3_Q1
11	V\$ETF_Q6
12	V\$CRX_Q4
13	VSAR_Q3
14	TGACCTTG_V\$SF1_Q6
15	V\$PAX8_Q1

Fig 11. GSEA identified pathways suppressed in Pten/Smad4-deficient tumors

isolated and subjected to microarray analysis. As expected, tumor and stroma showed distinct expression pattern by Hierarchical Clustering Analysis (Figure 10), and IPA indicated that while tumor cells are enriched for pathways involving cell adhesion molecules and tight junction (consistent with their epithelial nature), stromal cells display activation of more diverse signaling pathways involved in chronic inflammation, such as cytokine/cytokine

B



Results:

1. Transcriptomic profiling of GFP+ tumor cells and Tomato+ stromal cells from *Pten*^{pc/-} *Smad4*^{pc/-} shows a distinct expression pattern for these two populations. We isolated GFP+ tumor cells and Tomato+ stromal cells, from which RNAs were

receptor interaction, chemokine signaling pathway, Jak-STAT pathway, TCR pathway, and BCR pathway ($p < 0.01$, data not shown).

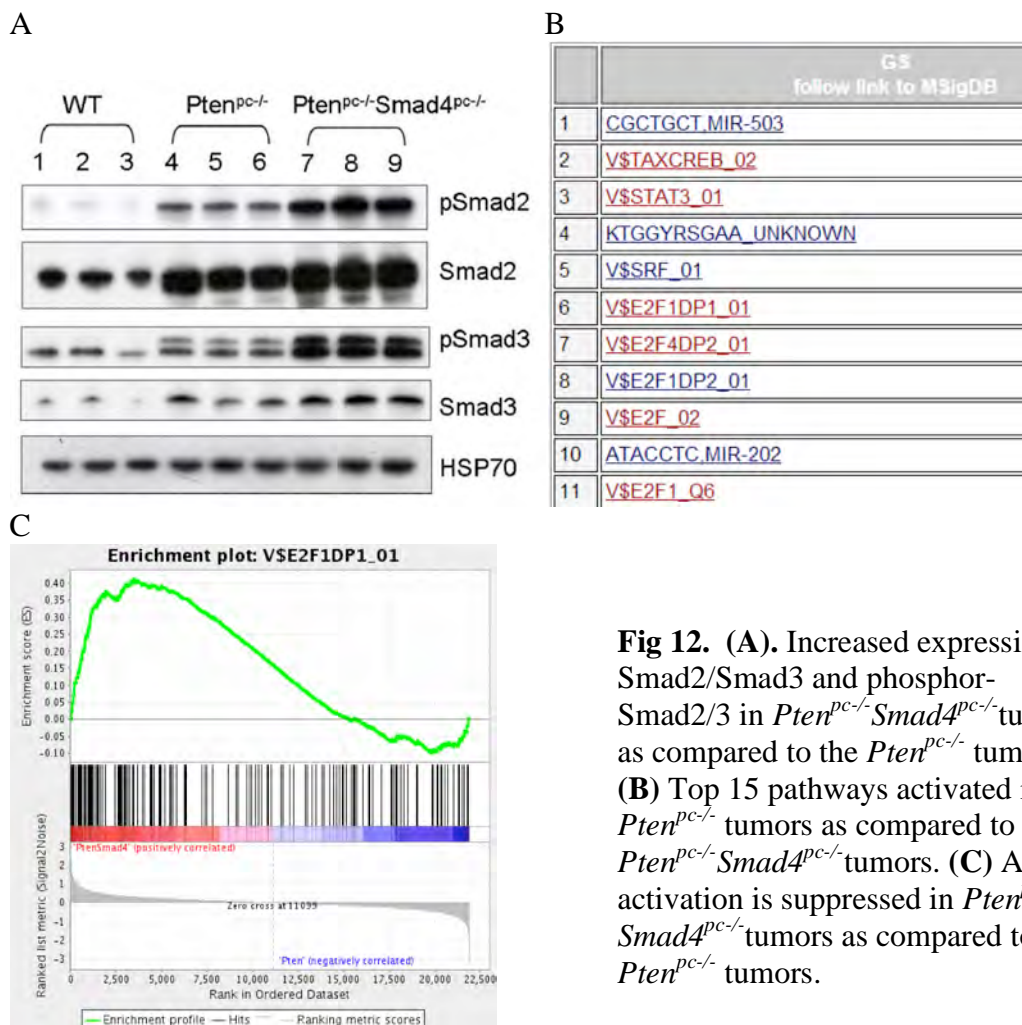


Fig 12. (A). Increased expression of Smad2/Smad3 and phosphor-Smad2/3 in *Pten^{pc/pc} Smad4^{pc/pc}* tumors as compared to the *Pten^{pc/pc}* tumors. **(B)** Top 15 pathways activated in *Pten^{pc/pc}* tumors as compared to the *Pten^{pc/pc} Smad4^{pc/pc}* tumors. **(C)** AR activation is suppressed in *Pten^{pc/pc} Smad4^{pc/pc}* tumors as compared to the *Pten^{pc/pc}* tumors.

2. Integrative transcriptomic analysis identified tumor and stroma specific genes which may play a role in CRPC and cancer stem cells. I performed an integrative analysis of our published dataset GSE25140 (*Pten^{pc/pc} Smad4^{pc/pc}* vs. *Pten^{pc/pc}*) and my new dataset (tumors vs. stroma (Tomato+)).

(1) Ar activity is suppressed in *Pten/Smad4* tumors as compared to *Pten* (Fig 11) as shown by Gene Enrichment Analysis (GSEA). This pathway is identified as the top pathways when compared *Pten^{pc/pc} Smad4^{pc/pc}* to *Pten^{pc/pc}*, which is in line with the histopathological findings described previously. Given the potential cross-talk between Tgfbeta/Smads pathways with AR signaling as Smad4 and Smad3 can interact with AR, it's possible that loss of Smad4 leads to a reprogramming of AR signaling pathways which renders the *Pten^{pc/pc} Smad4^{pc/pc}* tumors less dependent on AR signaling in ADT. Interestingly, total Smad3/Smad2 and phosphor-Smad2/3 expression are increased in *Pten/Smad4* as compared to *Pten* tumors.

- (2) Rb/E2Fs pathways are deregulated in the *Pten*^{pc/-}*Smad4*^{pc/-} tumors as compared to the *Pten*^{pc/-} tumors (Fig 12 B-C). Rb/E2Fs pathway deregulation has been shown to play an important role in human CRPC[8]. Interestingly, GSEA analysis identified multiple E2Fs signatures as the top 15 activated pathways in the *Pten*^{pc/-}*Smad4*^{pc/-} tumors as compared to the *Pten*^{pc/-} tumors, which is in line with the de novo resistance to ADT observed in the *Pten*^{pc/-}*Smad4*^{pc/-} tumors as compared to the *Pten*^{pc/-} tumors.
- (3) YAP1 is activated in the *Pten*^{pc/-}*Smad4*^{pc/-} tumors as compared to the *Pten*^{pc/-} tumors. In

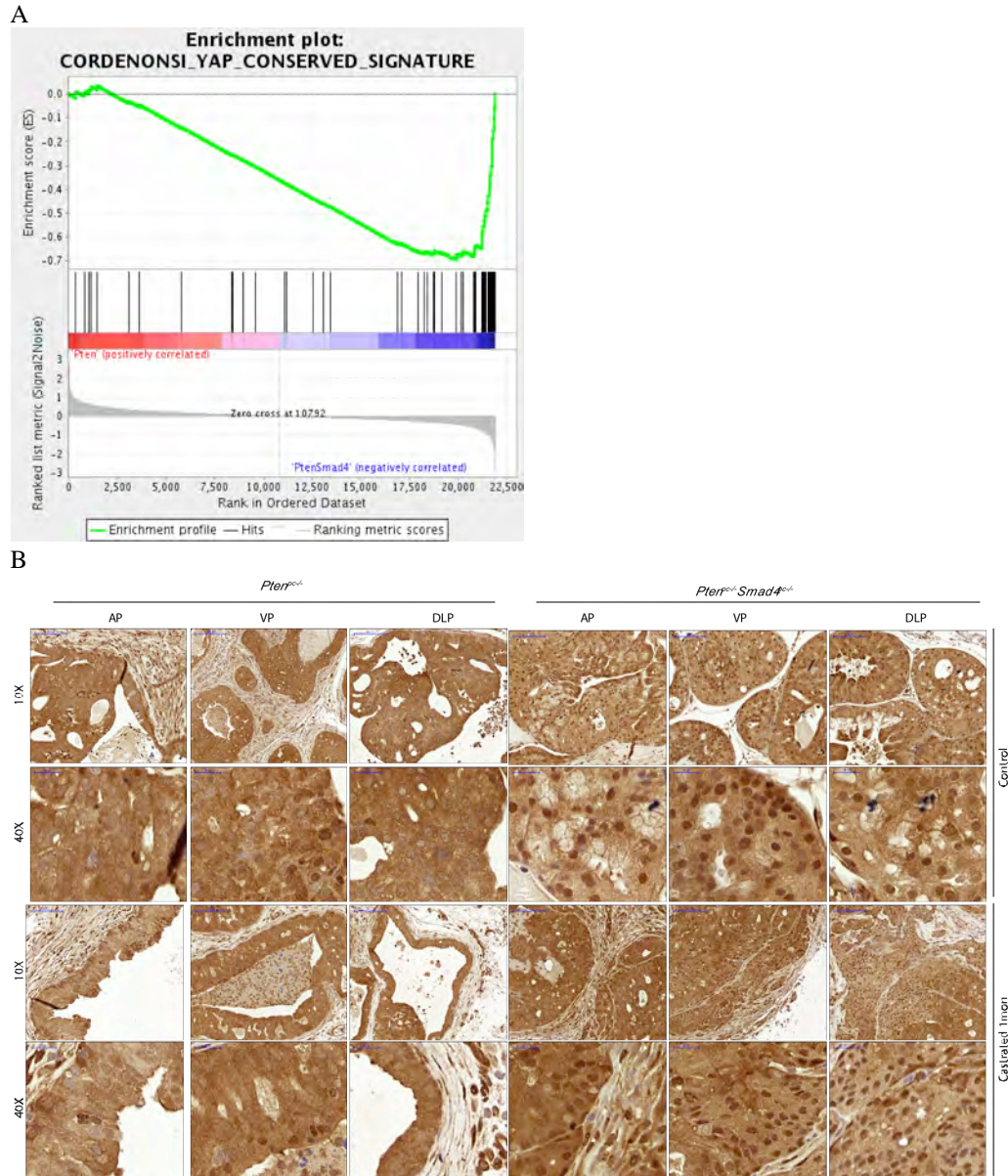


Fig. 13. YAP1 pathway may play a role in the de novo resistance to ADT in the *Pten*^{pc/-}*Smad4*^{pc/-} tumors. **(A)** YAP1 signature identified in the *Pten*^{pc/-}*Smad4*^{pc/-} tumors as compared to the *Pten*^{pc/-} tumors. **(B)** IHC staining of YAP1 in treatment naïve and castrated mice shows an increase in nuclear of YAP1 in *Pten*^{pc/-}*Smad4*^{pc/-} tumors as compared to *Pten*^{pc/-} tumors.

In addition to the Rb/E2Fs pathways, a novel pathway, Hippo/YAP1, is identified as one of the

top 10 activated oncogenic pathway signatures (GSEA C6 category, Fig 13 A). Although it is known that the Hippo–YAP pathway plays an important role in development and cancer in organs such as the liver, skin, intestine, and pancreas, the role for the Hippo–YAP pathway in prostate cancer biology is emerging [9-11]. Consistent with the *in silico* analysis, IHC analysis demonstrated a dramatic increase in the nuclear localization of Yap1 in *Pten^{pc/-}Smad4^{pc/-}* cancer cells as compared to *Pten^{pc/-}* cancer cells (Figure 6B). In addition, unbiased oPOSSUM analysis [12] indicated that TEAD1, a member of the TEAD transcription factor family that is required for Yap1 function, ranked second among the top ten transcription factors with over-represented binding sites in the 70 cancer-specific genes that were upregulated in the *Pten^{pc/-}Smad4^{pc/-}* tumors as compared to the *Pten^{pc/-}* tumors (≥ 1.5 fold, Z-Score=13.362, data not shown), an observation reinforcing the relevance of the Hippo–YAP pathway.

Furthermore, YAP1 remains highly expressed in CRPCs from *Pten^{pc/-}Smad4^{pc/-}* tumors as compared to the *Pten^{pc/-}* tumors (Fig 13B), suggesting that Hippo/YAP1 pathways may play a direct role in the de novo resistance to ADT for the *Pten^{pc/-}Smad4^{pc/-}* tumors. Given the role of YAP1 in stem cells[13, 14], it's possible that deregulation of Hippo/YAP1 pathways may play a role in the prostate cancer stem cells, which contribute to the observed CRPC phenotypes in *Pten^{pc/-}Smad4^{pc/-}* tumors.

Progress, accomplishment and discussion:

I have performed integrative analysis of our previous published microarray dataset GSE25140 & this tumor/stroma microarray dataset identified novel pathways that may play an important role in tumor progression, resistance to castration and cancer stem cells. Tumors from castrated mice and sham control mice will be subjected to RNA-seq analysis and additional candidate genes for CRPC and cancer stem cells will be subjected to functional validation in vitro and in vivo. In addition, I will continue to investigate the role of the novel Hippo/YAP1 pathway in the development of CRPC and cancer stem cells.

Key research accomplishments:

- Completed the Kaplan-Meier survival analysis of Pten/Smad4 mice with a large cohort.
- Comprehensive histopathological analysis of CRPC in the Pten/Smad4 mice suggests an expansion of the prostate tumor cells that express basal cell markers, such as Ck5 and p63. These basal type CRPC cells are highly proliferative, suggesting it may contain the cancer stem cell population.
- Transcriptome profiling of GFP+ tumor cells and Tomato+ cells from my refilled Pten/Smad4/mTmG model identified tumor- and stroma-specific genes and pathways
- Integrative analysis of our published microarray dataset GSE25140 and the new Pten/Smad4 tumor/stroma dataset identified novel pathways that may play an important role in prostate cancer progression, metastasis, and resistance to ADT and resistance to MDV3100, such as Rb/E2Fs, AR, and Hippo/YAP1 pathways.

Aim 3. Functional validation of CRPC genes in cancer stem cells.

Current objects: (a) Functional validation of the role for Yap1 in prostate cancer progression and castration resistance. (b) Functional validation of the role for Sox2 in prostate cancer progression and castration resistance. (c) Characterization of the role of myeloid-derived suppressor cells in prostate cancer progression and castration resistance.

Methodology: We overexpressed Yap1 and Sox2 or knockdown the expression of Yap1 and Sox2 in mouse prostate cancer cell lines. These cell lines were subjected to in vitro proliferation and subcutaneous xenograft. In addition, we performed CyTOF, a mass-

spectrometry approach to perform immunophenotyping at a single cell level cells[15, 16]. Mass Cytometry, also named CyTOF, uses antibodies labeled with rare element isotopes in mass spectrometric analysis of single cells and can simultaneously measure over 40 markers for a high dimensional single cell analysis of cell identity, clinical biomarkers, signaling proteins, transcription factors, proliferation, and apoptosis. Comparing to FACS, there is no compensation and no auto-fluorescence in CyTOF that might obscure weak signals. The immune suppressive activities of MDSCs were tested by an established in vitro T cell proliferation assay. The role of MDSCs were investigated by pharmacological depletion of MDSCs with anti-Gr1 antibody (clone RB6-8C5) [17], and Pep-H6 peptide-Fc fusion protein which binds specific to MDSCs [18].

Results:

1. Yap1 is regulates cell proliferation and tumor growth in $Pten^{pc/-} Smad4^{pc/-}$ prostate tumors. We validated the role of Yap1 in prostate tumorigenesis using in vitro and ex vivo assay. Specifically, we knockdowned the expression Yap1 by two doxycycline-inducible shRNAs (Fig. 14A) in a $Pten/Smad4/p53$ syngeneic cell line (B6 background). We demonstrated that knockdown of Yap1 not only significantly reduced the cell proliferation in vitro (data not shown), but also the tumor growth in immune competent mice (Fig. 14 B).

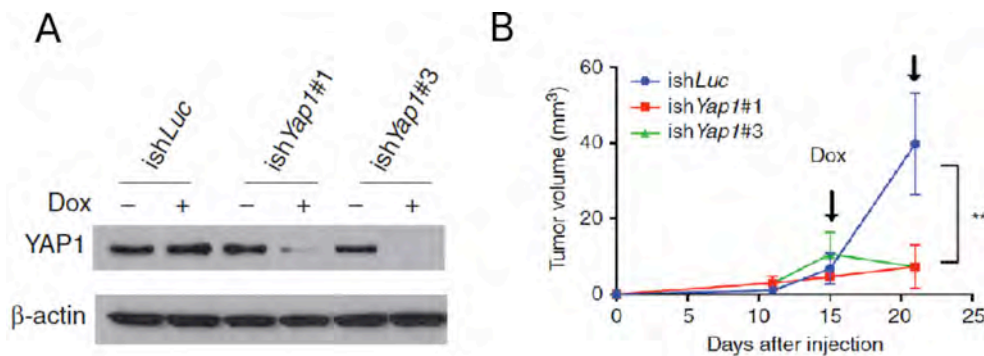


Fig. 14. Yap1 knockdown suppresses tumor growth. (A) Western blot for Yap1 knockdown by shRNA. (B). SubQ tumor growth for prostate cancer cells infected with inducible Yap1 shRNAs and control shRNA.

2. Sox2 is hyperactivated in $Pten^{pc/-} Smad4^{pc/-}$ prostate tumors. Similarly, GSEA analysis identified Sox2 activation signature in the $Pten^{pc/-} Smad4^{pc/-}$ prostate tumors as compared to the $Pten^{pc/-}$ prostate tumors (Fig. 15A). It has been shown that Sox2 is required for the tumorigenesis of the Rb1-deficient cells and Sox2 directly regulates Yap1 expression in the osteoprogenitors and MSCs [19]. We demonstrated that Sox2 is not expressed in the luminal cells in the wild type prostates and its expression is increased in $Pten^{pc/-}$ and $Pten^{pc/-} Smad4^{pc/-}$ tumors. However, the expression of Sox2 in $Pten^{pc/-} Smad4^{pc/-}$ tumors is much higher than that in $Pten^{pc/-}$ tumor (Fig. 15B-D). In addition, Sox2 remains highly expressed in the CRPCs from the $Pten/Smad4$ -deficient tumors (Fig. 15E). Importantly, shRNA knockdown of the Sox2 in castration resistant $Pten/Smad4$ -deficient cancer cell lines significantly decrease their proliferation, supporting the notion that Sox2 may play a role in the cancer stem cells and castration resistance.

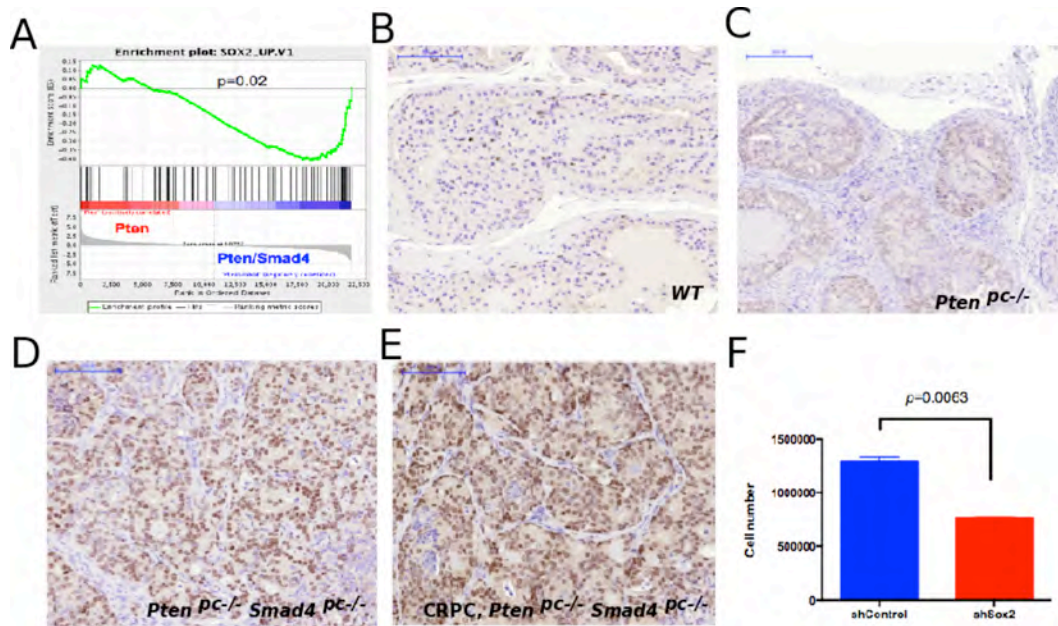


Fig. 15. Sox2 may play a role in cancer stem cells and castration resistance. (A) GSEA identified Sox2 activation signature in *Pten*/*Smad4*-deficient tumors. (B-E) Sox2 expression in wild type prostate (B), *Pten*-deficient prostate tumors (C), hormone naïve (D) and castration resistant (E) tumors from *Pten*/*Smad4* mice. (F) shRNA knockdown of Sox2 decreased the proliferation of the *Pten*/*Smad4*-deficient cancer cells.

3. Immune suppressive myeloid-derived suppressor cells (MDSCs) are the major infiltrated immune cells in *Pten*^{pc-/}*Smad4*^{pc-/} prostate tumors. We performed flow cytometry and found that infiltrated immune cells, particularly CD11b⁺ myeloid cells, are significantly increased in *Pten*^{pc-/}*Smad4*^{pc-/} prostate tumors as compared to the *Pten*^{pc-/} prostate tumors (Fig. 16A-B). We then perform CyTOF analysis and identified CD11b⁺Gr1⁺myeloid-derived suppressor cells (MDSCs) are the major infiltrated immune cells in the hormone naïve mouse prostate tumors (Fig. 16C). In addition, we observed that castration significantly increase the total number of tumor-infiltrated MDSCs (Fig. 16D). We also demonstrated that the MDSCs isolated from *Pten*^{pc-/}*Smad4*^{pc-/} prostate tumors are immune suppressive, as they can potently suppress the T cell proliferation in vitro (Fig. 16E). Given that MDSCs have been demonstrated to play an important role in immune suppression, angiogenesis, and metastasis, it's possible that MDSC may be involved in castration resistance and cancer stem cell niche[20].

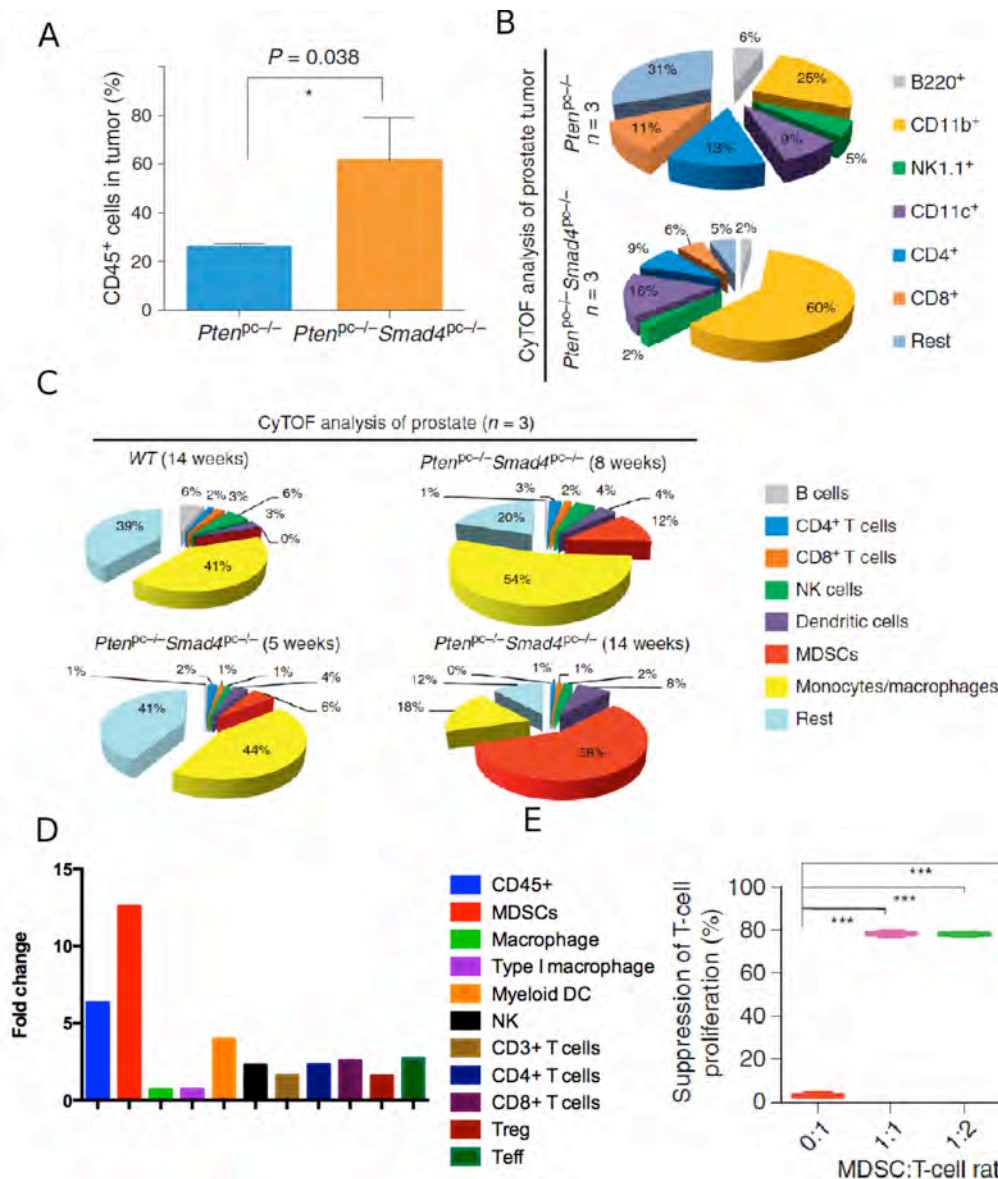


Fig. 16. Immune suppressive MDSCs are the major immune cell populations in the *Pten/Smad4*-deficient prostate tumors. (A-B) CyTOF demonstrated that *Pten/Smad4*-deficient tumors have more CD45⁺ cells (A) and CD11b⁺ myeloid cells (B). (C) CD11b⁺Gr1⁺ MDSCs are the major immune cells populations in invasive *Pten/Smad4*-deficient tumor (14 weeks) and is increased during tumor progression. (D) Castration induced a massive increase in CD45⁺ cells, and MDSCs are the immune cells have the max increase. (E) MDSCs possess potent immune suppressive activities.

4. MDSCs play an important role in prostate cancer progression and castration resistance. Given the abundance of MDSCs in the *Pten/Smad4*-deficient prostate tumors, we tested whether depletion of MDSCs affect tumor progression. We demonstrated that Gr1 antibody treatment, which depletes Gr1⁺ MDSCs, resulted in delayed tumor progression (Fig. 17A). In addition, Pep-H6 peptide-Fc fusion protein, which specifically target the MDSCs [18] resulted in a dramatic tumor regression after treatment for 4 months (Fig. 17B) and extended overall

survival of *Pten*/*Smad4* mice (Fig. 17C). Importantly, Pep-H6 peptibody and castration resulted in a dramatic tumor in 8 weeks as compared the Pep-H6 peptibody treatment (Fig. 17D), suggesting that MDSCs may also play a role in castration resistance.

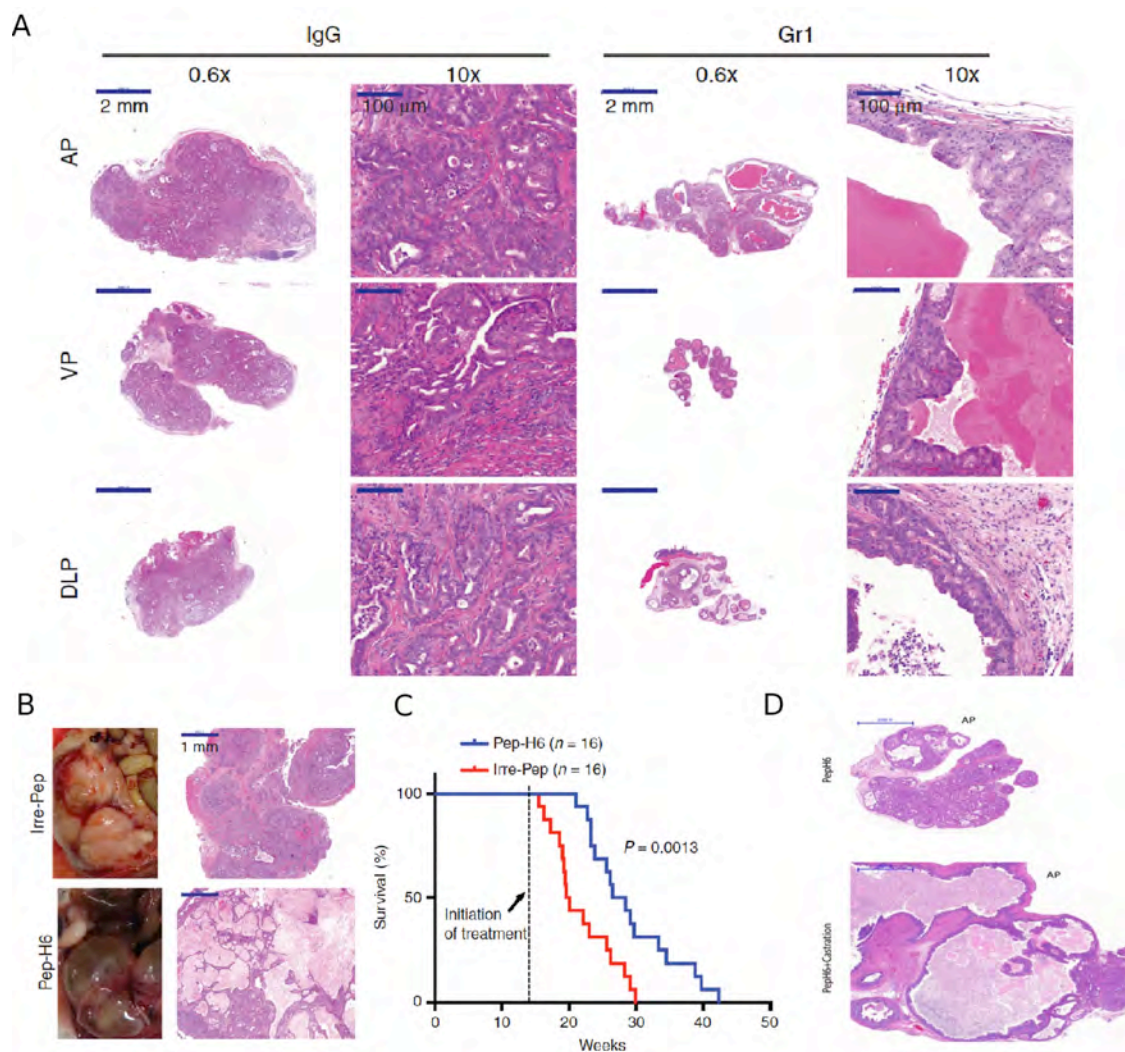


Fig. 17. MDSCs play an important role in tumor progression and castration resistance. (A) MDSC depletion by Gr1 antibody significantly delayed tumor progression. **(B)** Pep-H6 peptibody treatment resulted in tumor regression and extended overall survival. **(C)** Pep-H6 peptibody treatment in combination with castration resulted in dramatic tumor regression as compared to the castration alone.

5. Yap1-Cxcl5-Cxcr2 axis regulates MDSCs recruitment. To understand the molecular mechanisms underlying the massive infiltration of MDSCs in the *Pten*/*Smad4*-deficient prostate tumors, we performed transcriptome analysis of the GFP⁺ tumor cells and tdTomato⁺ stromal cells using the dual reporter mice we generated as described above (*Pb-Cre*, *Pten*^{L/L}, *Smad4*^{L/L}, *mTmG*^{L/+}). We identified Cxcl5 as the most significantly increased chemokine in the *Pten*/*Smad4*-deficient tumor cells as compared to the *Pten*-deficient tumor cells (data not shown). We confirmed this finding by immunohistochemical staining (Fig. 18A). In addition, we demonstrated Cxcl5 and Cxcr2 axis play an important role in the MDSCs in vitro migration (Fig. 18B) using neutralizing antibody or small molecular inhibitor for Cxcl5 and

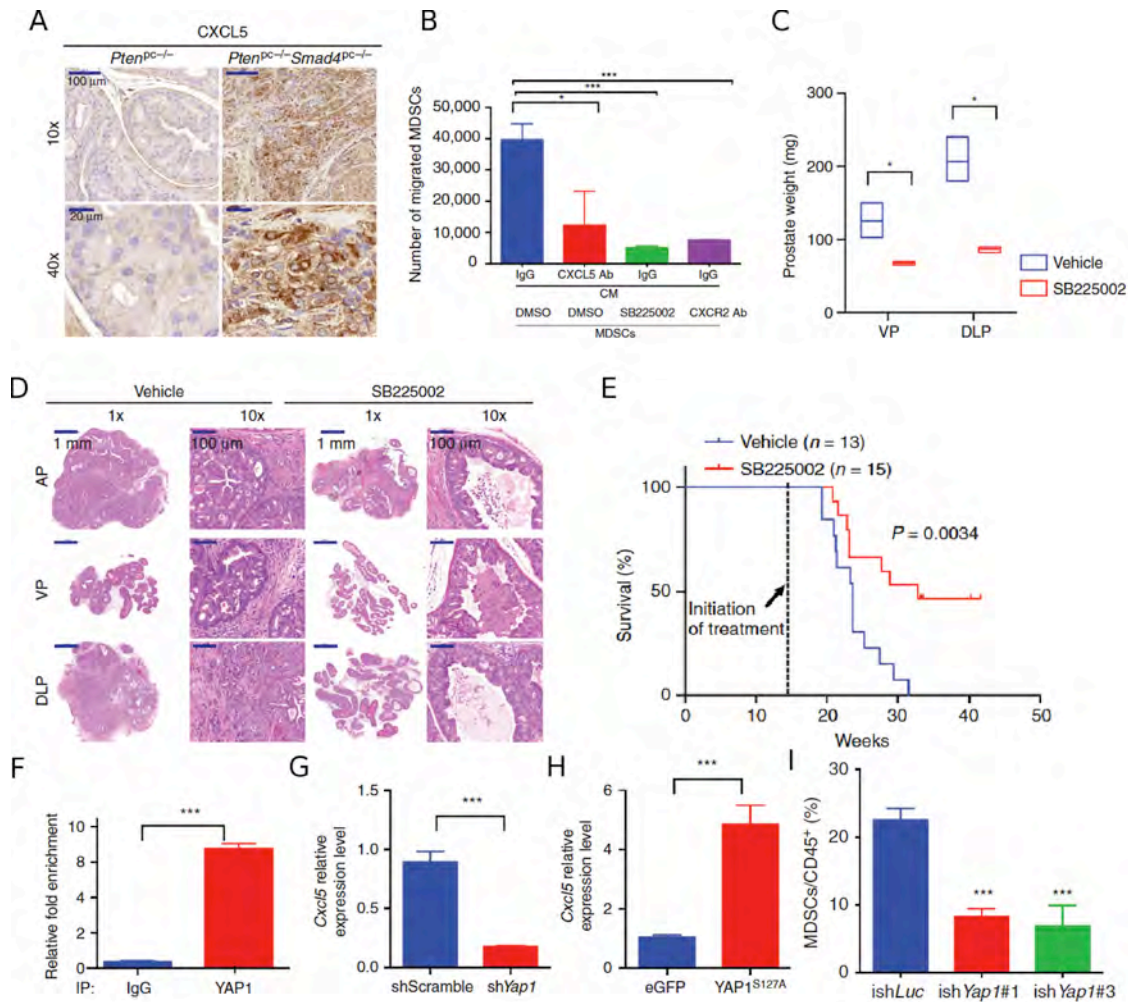


Fig. 18. Yap1-Cxcl5-Cxcr2 axis regulates MDSCs recruitment and tumor progression. (A) Cxcl5 expression in *Pten*/*Smad4*-deficient tumors and *Pten*-deficient tumors. (B) Cxcl5-Cxcr2 axis regulates MDSC migration in vitro. (C-E) Blocking MDSCs trafficking by Cxcr2 inhibitor SB225002 delayed tumor progression and extended overall survival of *Pten*/*Smad4* mice. (F) Yap1 binds to Cxcl5 promote as show by ChIP. (G-H) Yap1 regulates Cxcl5 transcription. (I) knockdown of Yap1 resulted in reduced MDSCs infiltration in vivo.

Cxcr2. In vivo treatment of *Pten*/*Smad4* mice significantly delayed the tumor progression and extended the overall survival (Fig. 18C-E). Given that Yap1 is hyperactivated in *Pten*/*Smad4*-deficient prostate tumors, we tested whether Yap1, a transcriptional coactivator, could directly regulate the transcription of Cxcl5. Indeed, Yap1 directly binds to Cxcl5 promotes as shown by chromatin-immunoprecipitation (ChIP) (Fig. 18F) and regulates Cxcl5 transcription as shown by overexpression of constitutive active Yap1 S127A mutant or knockdown of Yap1 by shRNA (Fig. 18G-H). Lastly, inducible knockdown of Yap1 expression in significantly reduced the infiltration of MDSCs in a subQ xenograft model (Fig. 18I).

6. Expression of Yap1 and Sox2 in human prostate cancer. Since we have demonstrated a role for Yap1 and Sox2 in tumor progression in mice, we tested whether they are also deregulated in human prostate cancer. First we examined the expression of Yap1 in human prostate cancer by tissue microarray analysis (TMA). We demonstrated that Yap1 is not expressed in the luminal cells of normal human prostate, but is overexpressed in a subset of human prostate cancer (Fig. 19A-B). To determine whether Yap1 also regulates MDSCs recruitment in human, we performed hierarchical clustering of RNA-seq data from TCGA prostate cancer

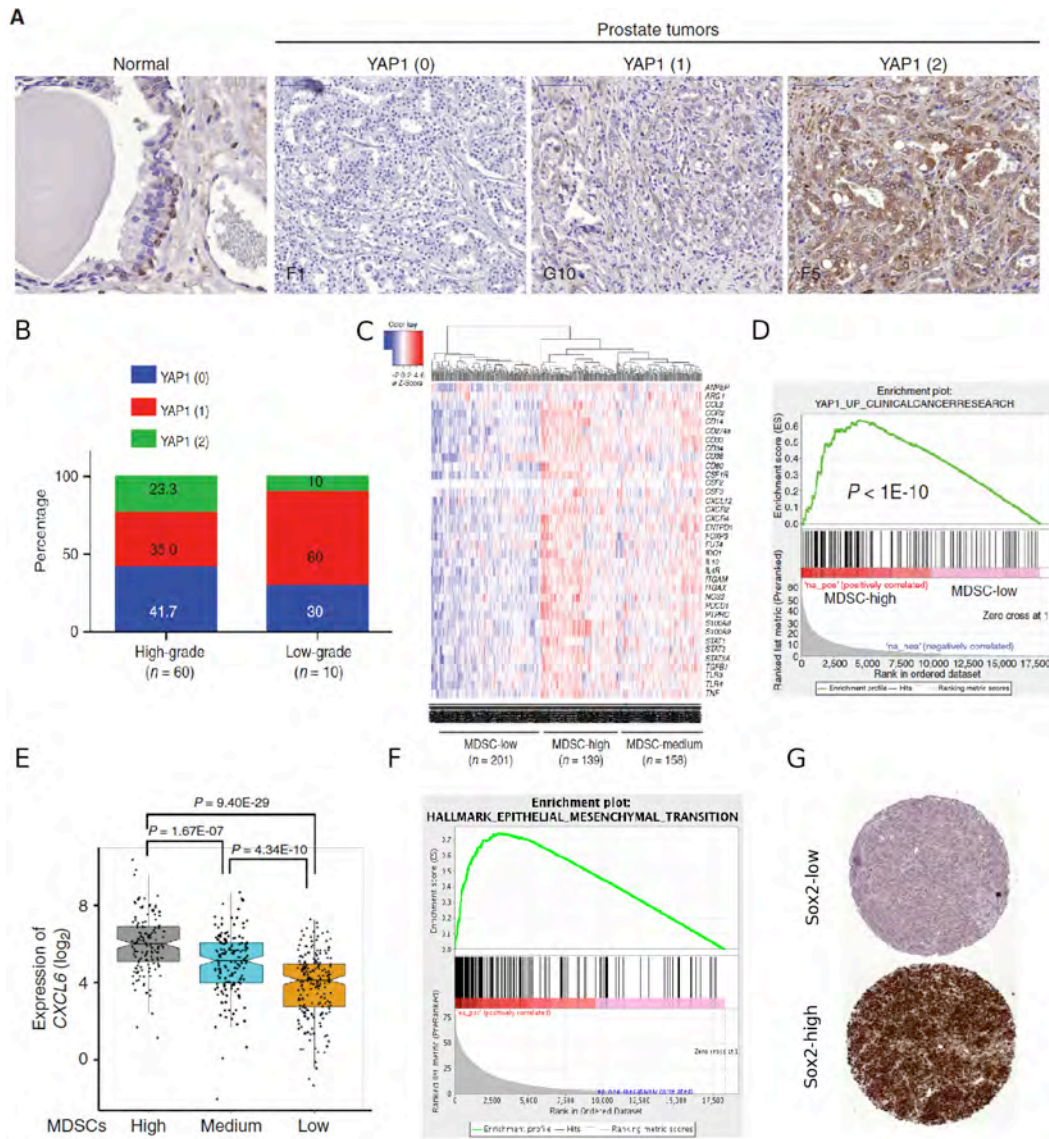


Fig. 19. Yap1 and Sox2 in human prostate cancer. (A-B) Yap1 expression in human prostate cancer as shown by IHC. (C) MDSC signature clusters TCGA prostate tumor samples into three groups. (D) Yap1 signature was identified in MDSC-high group. (E) Cxcl6 is highly expressed in MDSC-high group. (F) EMT signature was identified in Yap1-activated TCGA prostate tumor samples. (G) Sox2 is highly expressed in a subset of human CRPC.

samples using a MDSC-signature with 39 genes. We demonstrated that human prostate cancer samples can be classified into three groups, MDSC-high, MDSC-low, MDSC-medium (Fig. 19C). Importantly, Yap1 is hyperactivated in MDSC-high group as compared to MDSC-low group (Fig. 19D-E) and Cxcl6, the human homologue of mouse Cxcl5, is highly expressed in MDSC-high group, which is in line with our findings in mice. Furthermore, EMT signature is identified in Yap1 activated TCGA prostate tumor samples (Fig. 19F), suggesting that Yap1-Cxcl5-Cxcr2 axis and MDSCs may also regulate cancer stem cell and metastasis. Lastly, we also demonstrated Sox2 is highly expressed in a subset of human CRPC samples by TMA analysis (Fig. 19G)

Progress, accomplishment and discussion: Through transcriptome analysis, I identified Yap1 and Sox2 as potential regulator of prostate cancer progression and castration resistance. In addition, I established a Yap1-Cxcl5-Cxcr2 in the regulation of the recruitment of immune suppressive MDSCs in prostate cancer. I also demonstrated that targeting MDSCs could an effective approach for advanced prostate cancer.

Key research accomplishments:

- Identification of myeloid-derived suppressor cells (MDSCs) as the major infiltrated immune cells in the Pten/Smad4 tumors.
- Demonstration the critical role for MDSCs in prostate cancer progression.
- Established a Yap1-Cxcl5-Cxcr2 axis in the regulation of MDSCs recruitment, which could also function in human prostate cancer, as shown by the analysis of TCGA prostate cancer RNA-seq data using a MDSC-signature.

3C. What opportunities for training and professional development has the project provided?

1) Training from intra- and inter-laboratory interactions: I cannot ask for a better training environment than DePinho lab. This project has provided me with ample opportunities for me to interact with not only the members of the DePinho laboratory, but also experts in cancer research within MD Anderson Cancer Center and experts from other institutions. We have weekly lab meeting and journal club with post-docs and graduate students from Ron DePinho, Lynda Chin and Giulio Draetta labs, which provide great opportunities to present my work in a critical academic setting and to learn about emerging discoveries from other talented post-docs and graduate students. Since Dr. DePinho took the position of President of MDACC, I was exposed to a whole array of facilities and cores, and I've got the chance to talk to some of the directors who are willing to assist me in different aspects of my research. In addition, I have maintained a good relationship with bioinformaticians and biostatisticians led by Dr. Chin and the scientists from the Institute of Applied Cancer Science led by Dr. Draetta. By collaborating and exchanging ideas with these scientists and physicians, I not only benefit from their great science, but will also build up a strong network for my future independent career.

2) Grant writing: With the help of Drs. DePinho and Chin, I successfully got the Department of Defense Prostate Cancer Research Program Postdoctoral Training Award. In addition, I'm helping Dr. DePinho to put together a CIPRIT grant on the novel prostate cancer mouse model generated in our lab. These experiences are invaluable, as Dr. DePinho will work closely with me to make sure I learn and understand the craft of grant writing.

3) Scientific communication in writing: I'm working closely with Dr. DePinho in writing my first-author research article on the novel molecular mechanisms for CRPC in the Pten/Smad4 mouse model. I worked closely with Dr. DePinho in the writing of my recent publication in Cancer Discovery.

4) Scientific communication in speaking: I routinely present my work in the DePinho lab meeting every other month in MDACC. I also regularly present my work in the joined weekly lab meeting among Draetta lab/Chin lab/DePinho lab/IACS and in the weekly Cancer Biology Department Seminar. In addition, I present regularly in the weekly Department of Cancer Biology Journal club. Moreover, I presented my work on the Yap1-dependent MDSCs recruitment in prostate cancer progression in SITC 2015 during the poster session. I believe these training activities will make presentation skill one of my strengths and help me interview for and attain a faculty position.

5) Lab management/Mentoring training: The DePinho lab is big, so all of the post-docs participate heavily in ensuring that various aspects of the lab are running smoothly. Finally, I will continue to learn from Dr. DePinho, who is a master of mentoring himself, to improve a wide range of skills on mentoring and management.

6) Seminar series/Conferences/Workshops: MD Anderson Cancer Center offer a wide range of top-notch seminars/series/conferences, where I keep abreast of current research findings around the world. I presented my work in the annual postdoc symposium at MD Anderson Cancer Center and received AMGEN Award for Basic Science Research in 2015.

3D. How were the results disseminated to communities of interest?

Nothing to Report

3E. What do you plan to do during the next reporting period to accomplish the goals?

Nothing to Report

4. IMPACT

4A. What was the impact on the development of the principal discipline(s) of the project?

We have demonstrated that ADT in *Pten^{pc/-}Smad4^{pc/-}* mice promoted lung metastasis, which is consistent with the literature that ADT could promote epithelial-mesenchymal transition. This would suggest that we have to understand the context in which ADT promotes EMT and the molecular mechanisms underlying this process. In addition, we demonstrated first time in the lethal murine prostate cancer model that Yap1-dependent myeloid-derived suppressor cells (MDSCs) could serve as an effective therapeutic target for advanced prostate cancer. Further studies of the role of MDSCs in human prostate cancer may lead to new clinical trial to target these immune suppressive cells. In addition, I also demonstrated that Sox2 may play an important role in the development of prostate cancer progression and castration resistance. The understanding of the molecular mechanisms for the role of Sox2 in prostate cancer may lead to the development of novel therapy for CRPCs.

4B. What was the impact on other disciplines?

Nothing to Report.

4C. What was the impact on technology transfer?

Nothing to Report.

4D. What was the impact on society beyond science and technology?

Nothing to Report.

5. CHANGES/PROBLEMS: Nothing to Report

6. Products:

6A. Publications, conference papers, and presentations

(1) Journal publication:

Author(s): Guocan Wang*, Xin Lu*, Prasenjit Dey, Pingna Deng, Chia Chin Wu, Shan Jiang, Zhuangna Fang, Kun Zhao, Ramakrishna Konaparthi, Sujun Hua, Jianhua Zhang,

Elsa M. Li Ning Tapia, Avnish Kapoor, Chang-Jiun Wu, Neelay Bhaskar Patel, Zhenglin Guo, Vandhana Ramamoorthy, Trang N. Tieu, Tim Heffernan, Di Zhao, Xiaoying Shang, Sunada Khadka, Pingping Hou, Baoli Hu, Xiaolu Pan, Zhihu Ding, Yanxia Shi, Liren Li, Edward Chang, Patricia Troncoso, Christopher J. Logothetis, Mark McArthur, Lynda Chin, Y. Alan Wang, Ronald A. DePinho;

Title: Targeting YAP-dependent MDSC infiltration impairs tumor progression

Journal: *Cancer Discovery*; January 1, 2016 6; 80;

Status of publication: published;

Acknowledgement of federal support: Yes

6B. Website(s) or other Internet site(s)

(1) Cancer Frontline provides the professional health community with the latest information about MD Anderson's cancer fighting efforts.

<http://www.cancerfrontline.org/category/translational-cancer-research/>

(2) Medical Xpress is a web-based medical and health news service that is part of the renowned Science X network.

<http://medicalxpress.com/news/2015-12-immune-suppressor-cells-advanced-prostate.html>

(3) ScienceDaily is one of the Internet's most popular science news web sites. Since starting in 1995, the award-winning site has earned the loyalty of students, researchers, healthcare professionals, government agencies, educators and the general public around the world.

<https://www.sciencedaily.com/releases/2015/12/151221133834.htm>

7. PARTICIPANTS & OTHER COLLABORATING ORGANIZATIONS

7A. What individuals have worked on the project?

Name:	Guocan Wang
Project Role:	PI
Researcher Identifier (e.g. ORCID ID):	n/a
Nearest person month worked:	24
Contribution to Project:	Dr. Guocan Wang has designed the experiments and performed most of work in this project.
Funding Support:	USAMRMC W81XWH-13-1-0202

Name:	Konaparthi Ramakrishna
Project Role:	Graduate Student
Researcher Identifier (e.g. ORCID ID):	n/a
Nearest person month worked:	5

Contribution to Project:	Mr. Ramakrishna assisted Dr. Wang in mouse genotyping, immunohistochemistry, and qPCR.
Funding Support:	Dr. DePinho's startup fund from MD Anderson Cancer Center

7B. Has there been a change in the active other support of the PD/PI(s) or senior/key personnel since the last reporting period?

Nothing to Report

7C. What other organizations were involved as partners?

Nothing to Report

8. SPECIAL REPORTING REQUIREMENTS

N/A

9. APPENDICES

9A. List of references

1. Jemal, A., et al., *Cancer Statistics, 2010*. CA: A Cancer Journal for Clinicians, 2010. **60**(5): p. 277-300.
2. Bubley, G.J. and S.P. Balk, *Treatment of Androgen-Independent Prostate Cancer*. Oncologist, 1996. **1**(1 & 2): p. 30-35.
3. Attard, G., et al., *Selective inhibition of CYP17 with abiraterone acetate is highly active in the treatment of castration-resistant prostate cancer*. J Clin Oncol, 2009. **27**(23): p. 3742-8.
4. Tran, C., et al., *Development of a second-generation antiandrogen for treatment of advanced prostate cancer*. Science, 2009. **324**(5928): p. 787-90.
5. Kang, H.Y., et al., *Differential modulation of androgen receptor-mediated transactivation by Smad3 and tumor suppressor Smad4*. J Biol Chem, 2002. **277**(46): p. 43749-56.
6. Lunardi, A., et al., *A co-clinical approach identifies mechanisms and potential therapies for androgen deprivation resistance in prostate cancer*. Nat Genet, 2013. **45**(7): p. 747-55.
7. Wang, G., et al., *Zbtb7a suppresses prostate cancer through repression of a Sox9-dependent pathway for cellular senescence bypass and tumor invasion*. Nat Genet, 2013. **45**(7): p. 739-46.
8. Sharma, A., et al., *The retinoblastoma tumor suppressor controls androgen signaling and human prostate cancer progression*. J Clin Invest, 2010. **120**(12): p. 4478-92.
9. Johnson, R. and G. Halder, *The two faces of Hippo: targeting the Hippo pathway for regenerative medicine and cancer treatment*. Nat Rev Drug Discov, 2014. **13**(1): p. 63-79.
10. Kapoor, A., et al., *Yap1 activation enables bypass of oncogenic Kras addiction in pancreatic cancer*. Cell, 2014. **158**(1): p. 185-97.
11. Shao, D.D., et al., *KRAS and YAP1 converge to regulate EMT and tumor survival*. Cell, 2014. **158**(1): p. 171-84.

12. Kwon, A.T., et al., *oPOSSUM-3: advanced analysis of regulatory motif over-representation across genes or ChIP-Seq datasets*. G3 (Bethesda), 2012. **2**(9): p. 987-1002.
13. Camargo, F.D., et al., *YAP1 increases organ size and expands undifferentiated progenitor cells*. Curr Biol, 2007. **17**(23): p. 2054-60.
14. Zhao, B., K. Tumaneng, and K.L. Guan, *The Hippo pathway in organ size control, tissue regeneration and stem cell self-renewal*. Nat Cell Biol, 2011. **13**(8): p. 877-83.
15. Bendall, S.C. and G.P. Nolan, *From single cells to deep phenotypes in cancer*. Nat Biotechnol, 2012. **30**(7): p. 639-47.
16. Chattopadhyay, P.K., et al., *Single-cell technologies for monitoring immune systems*. Nat Immunol, 2014. **15**(2): p. 128-35.
17. Pekarek, L.A., et al., *Inhibition of tumor growth by elimination of granulocytes*. J Exp Med, 1995. **181**(1): p. 435-40.
18. Qin, H., et al., *Generation of a new therapeutic peptide that depletes myeloid-derived suppressor cells in tumor-bearing mice*. Nat Med, 2014. **20**(6): p. 676-681.
19. Seo, E., et al., *SOX2 regulates YAP1 to maintain stemness and determine cell fate in the osteo-adipo lineage*. Cell Rep, 2013. **3**(6): p. 2075-87.
20. Condamine, T., et al., *Regulation of tumor metastasis by myeloid-derived suppressor cells*. Annu Rev Med, 2015. **66**: p. 97-110.

9B. Publication (Wang et al, Cancer Discovery, 2016)

RESEARCH ARTICLE

Targeting YAP-Dependent MDSC Infiltration Impairs Tumor Progression

Guocan Wang^{1,2}, Xin Lu^{1,2}, Prasenjit Dey^{1,2}, Pingna Deng^{1,2}, Chia Chin Wu³, Shan Jiang², Zhuangna Fang^{2,4}, Kun Zhao², Ramakrishna Konaparthi², Sujun Hua^{1,2}, Jianhua Zhang³, Elsa M. Li-Ning-Tapia⁵, Avnish Kapoor², Chang-Jiun Wu³, Neelay Bhaskar Patel², Zhenglin Guo¹, Vandhana Ramamoorthy³, Trang N. Tieu³, Tim Heffernan³, Di Zhao^{1,2}, Xiaoying Shang¹, Sunada Khadka¹, Pingping Hou^{1,2}, Baoli Hu^{1,2}, Eun-Jung Jin^{1,6}, Wantong Yao², Xiaolu Pan², Zhihu Ding⁷, Yanxia Shi^{2,4}, Liren Li^{2,4}, Qing Chang³, Patricia Troncoso⁸, Christopher J. Logothetis⁵, Mark J. McArthur⁹, Lynda Chin², Y. Alan Wang^{1,2}, and Ronald A. DePinho¹

ABSTRACT

The signaling mechanisms between prostate cancer cells and infiltrating immune cells may illuminate novel therapeutic approaches. Here, utilizing a prostate adenocarcinoma model driven by loss of *Pten* and *Smad4*, we identify polymorphonuclear myeloid-derived suppressor cells (MDSC) as the major infiltrating immune cell type, and depletion of MDSCs blocks progression. Employing a novel dual reporter prostate cancer model, epithelial and stromal transcriptomic profiling identified CXCL5 as a cancer-secreted chemokine to attract CXCR2-expressing MDSCs, and, correspondingly, pharmacologic inhibition of CXCR2 impeded tumor progression. Integrated analyses identified hyperactivated Hippo-YAP signaling in driving CXCL5 upregulation in cancer cells through the YAP-TEAD complex and promoting MDSC recruitment. Clinicopathologic studies reveal upregulation and activation of YAP1 in a subset of human prostate tumors, and the YAP1 signature is enriched in primary prostate tumor samples with stronger expression of MDSC-relevant genes. Together, YAP-driven MDSC recruitment via heterotypic CXCL5-CXCR2 signaling reveals an effective therapeutic strategy for advanced prostate cancer.

SIGNIFICANCE: We demonstrate a critical role of MDSCs in prostate tumor progression and discover a cancer cell nonautonomous function of the Hippo-YAP pathway in regulation of CXCL5, a ligand for CXCR2-expressing MDSCs. Pharmacologic elimination of MDSCs or blocking the heterotypic CXCL5-CXCR2 signaling circuit elicits robust antitumor responses and prolongs survival. *Cancer Discov*; 6(1); 80-95. © 2015 AACR.

INTRODUCTION

The tumor microenvironment (TME) is comprised of a complex mixture of tumor-associated fibroblasts, infiltrating immune cells, endothelial cells, extracellular matrix proteins, and signaling molecules, such as cytokines (1–3). Homotypic and heterotypic interactions between these cellular constituents play essential roles in cancer development and response to therapeutics (3, 4). Among the infiltrating immune cells, myeloid-derived suppressor cells (MDSC) represent a phenotypically heterogeneous population of immature myeloid cells that play a tumor-promoting role by maintaining a state of immunologic anergy and tolerance (5). In particular, activated MDSCs provide a source of secreted chemokines,

cytokines, and enzymes, which suppress local T-cell activation and viability (5). In addition, MDSCs can suppress T-cell activity through deprivation of nutrients, such as L-arginine and L-cysteine, and interference with T-cell receptor functions via reactive oxygen species (ROS) and reactive nitrogen species.

Prostate cancer is the most common noncutaneous malignancy in men in the United States. Similar to many other solid tumor types, prostate cancer is characterized by a rich tumor-stroma interaction network that forms the TME (1–3). In prostate cancer, various signaling pathways have been implicated in the cross-talk between tumor and stroma, such as androgen receptor signaling, FGF, SRC, TGF β , IGF, integrin, and Hedgehog pathways (1). Interestingly, MDSC abundance in the blood correlates with circulating PSA levels in patients with prostate cancer (6–8). MDSCs have been identified recently as a TME constituent in an indolent prostate cancer mouse model with conditional *Pten* deletion (9) and demonstrated to antagonize senescence during early tumorigenesis (10). However, the molecular mechanisms underlying the recruitment of MDSCs are not well understood, and the extent to which MDSCs facilitate prostate cancer progression has not been determined.

Previously, we have shown that deletion of *Pten* in the mouse prostate causes upregulation of SMAD4, which constrains cell proliferation and invasion, and, accordingly, dual deletion of *Pten* and *Smad4* results in rapid prostate cancer progression, including metastasis (11). Comparative transcriptomic and cell profile analyses of PTEN- versus PTEN/SMAD4-deficient prostate cancer revealed a prominent immune signature and resident MDSCs as a major TME population in PTEN/SMAD4-deficient tumors. Biologic, molecular, and pharmacologic analyses established that a YAP1-mediated CXCL5-CXCR2 signaling axis recruits MDSCs into the TME and that

¹Department of Cancer Biology, The University of Texas MD Anderson Cancer Center, Houston, Texas. ²Department of Genomic Medicine, The University of Texas MD Anderson Cancer Center, Houston, Texas. ³Institute for Applied Cancer Science, The University of Texas MD Anderson Cancer Center, Houston, Texas. ⁴Sun Yat-Sen University Cancer Center, Guangzhou, People's Republic of China. ⁵Department of Genitourinary Medical Oncology, The University of Texas MD Anderson Cancer Center, Houston, Texas. ⁶Department of Biological Science, College of Natural Sciences, Wonkwang University, Cheonbuk, Iksan, South Korea. ⁷Sanofi Oncology, Cambridge, Massachusetts. ⁸Department of Pathology, The University of Texas MD Anderson Cancer Center, Houston, Texas. ⁹Department of Veterinary Medicine and Surgery, The University of Texas MD Anderson Cancer Center, Houston, Texas.

Note: Supplementary data for this article are available at Cancer Discovery Online (<http://cancerdiscovery.aacrjournals.org/>).

G. Wang and X. Lu contributed equally to this article.

Corresponding Authors: Y. Alan Wang, The University of Texas MD Anderson Cancer Center, 1515 Holcombe Boulevard, Houston, TX 77030. Phone: 713-792-7928; Fax: 713-794-4005; E-mail: yalanwang@mdanderson.org; and Ronald A. DePinho, Phone: 713-792-6000, rdepinho@mdanderson.org

doi: 10.1158/2159-8290.CD-15-0224

© 2015 American Association for Cancer Research.

MDSCs play critical roles in facilitating tumor progression. Our comprehensive analyses using a prostate cancer model coupled with clinical validation using patient samples support the view that targeting either MDSC recruitment or infiltrated MDSCs may represent a valid therapeutic opportunity in treating advanced prostate cancer.

RESULTS

Prominent Infiltration of Immune Cells in the *Pten*^{pc/-}*Smad4*^{pc/-} Tumor Model

We previously reported that conditional deletion of *Smad4* bypassed the senescence barrier instigated by *Pten* loss in the prostate epithelia, resulting in a highly proliferative and invasive prostate adenocarcinoma characterized by an exuberant stromal reaction and frequent metastasis to distant organs (11). Correspondingly, ingenuity pathway analysis (IPA) revealed prominent representation of cell movement, cell proliferation, and antigen presentation as the top three categories represented in the *Pten*^{pc/-}*Smad4*^{pc/-} tumors (11). Further analysis revealed a prominent immune signature, including Granulocytes Adhesion and Diapedesis, Leukocytes Extravasation Signaling, and Agranulocytes Adhesion and Diapedesis as three of the top four most activated pathways in *Pten*^{pc/-}*Smad4*^{pc/-} tumors compared with those present in *Pten*^{pc/-} tumors (Fig. 1A; *P* value < 2.03E-7). Correspondingly, IHC staining highlighted conspicuous infiltration of CD45⁺ leukocytes in *Pten*^{pc/-}*Smad4*^{pc/-} tumors (Fig. 1B). To comprehensively audit the spectrum of infiltrating immune cells in tumors, we performed mass cytometry (CyTOF) immunophenotyping (12) to catalog tumor cell-type constituents from well-established tumors in 16-week-old *Pten*^{pc/-} and *Pten*^{pc/-}*Smad4*^{pc/-} mice. Employing a 9-marker antibody panel (Supplementary Table S1), CyTOF confirmed a significant increase in CD45⁺-infiltrating leukocytes in *Pten*^{pc/-}*Smad4*^{pc/-} as compared with *Pten*^{pc/-} tumors (Fig. 1C). Within the CD45⁺-infiltrating cells, CD11b⁺ myeloid cells represented a significantly increased immune population in *Pten*^{pc/-}*Smad4*^{pc/-} as compared with *Pten*^{pc/-} tumors (Fig. 1D).

CD11b⁺Gr1⁺ Cells Are Significantly Increased in *Pten*^{pc/-}*Smad4*^{pc/-} Tumor Model

To obtain a dynamic view of peripheral and infiltrating immune cells as a function of tumor progression in the *Pten*^{pc/-}*Smad4*^{pc/-} model, which initiates tumor development at 6 to 8 weeks and progresses to early invasive carcinoma by 14 weeks of age, serial CyTOF analyses using an expanded antibody panel of 17 surface markers (Supplementary Table S1) were performed on single cells from primary tumors, peripheral blood, spleen, and draining lymph nodes at 5, 8, and 14 weeks of age. The detailed immunophenotyping profiles enabled construction of the spanning-tree progression analysis of density-normalized events (SPADE)-derived tree (12). SPADE is a computational approach to facilitate the identification and analysis of heterogeneous cell types. SPADE of the *Pten*^{pc/-}*Smad4*^{pc/-} model displays the complexity of the TME, which is composed of epithelial tumor cells (EpCAM⁺CD45⁻), nonimmune TME cells (EpCAM⁺CD45⁻),

and infiltrating immune cells (EpCAM⁻CD45⁺) that can be further grouped into various immune cell subpopulations (Fig. 2A and Supplementary Fig. S1A). Among the infiltrating immune cells, there was a striking age-dependent increase of CD11b⁺Gr1⁺ cells in tumors (Fig. 2B) and peripheral blood from *Pten*^{pc/-}*Smad4*^{pc/-} mice (Fig. 2C); this trend was much less pronounced in the spleen or draining lymph nodes (Supplementary Fig. S1B; for gating strategy, see Supplementary Fig. S1C).

CD11b⁺Gr1⁺ Cells from *Pten*^{pc/-}*Smad4*^{pc/-} Tumors Are Potently Immunosuppressive

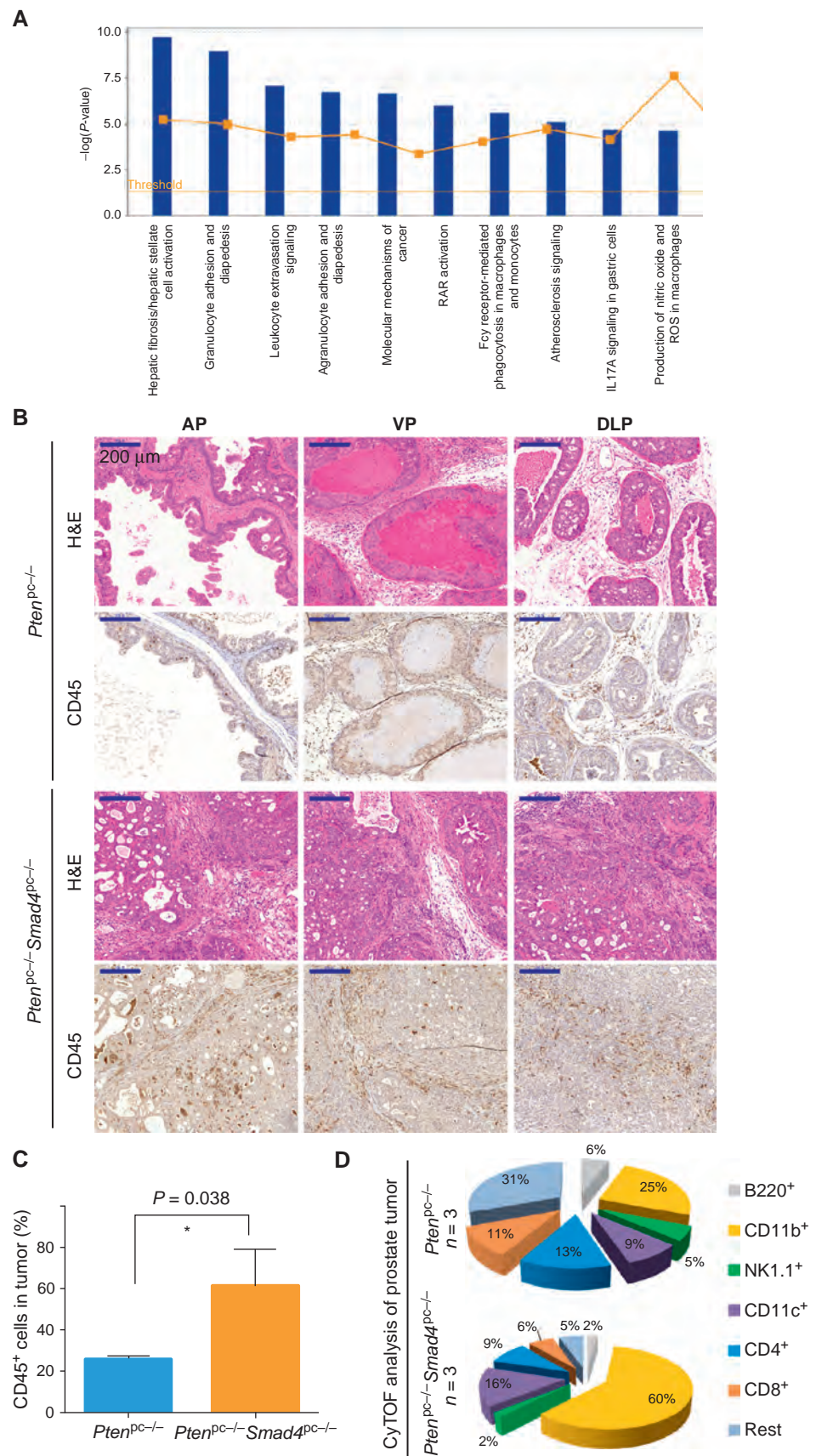
To evaluate the potential immunosuppressive activity of intratumoral CD11b⁺Gr1⁺ cells from *Pten*^{pc/-}*Smad4*^{pc/-} tumors, we examined T-cell proliferation using a standard cell coculture system. These CD11b⁺Gr1⁺ cells strongly suppressed CD3 and CD28 antibody-induced T-cell proliferation and activation (Fig. 3A and B; see Supplementary Fig. S2 for cell isolation strategy), establishing that CD11b⁺Gr1⁺ cells are indeed functional MDSCs.

MDSCs can be further classified as a Ly6G⁺Ly6C^{lo} subset with polymorphonuclear phenotype (PMN-MDSC) and a Ly6G⁻Ly6C^{hi} subset with monocytic phenotype (M-MDSC; ref. 13). PMN-MDSCs represented the major MDSC population in *Pten*^{pc/-}*Smad4*^{pc/-} tumors (Fig. 3C and D), consistent with previously observed preferential expansion of PMN-MDSCs in tumor-bearing mice of various syngeneic models (5, 9, 13). The abundance of PMN-MDSCs was further confirmed by IHC for Ly6G, as shown by quantification of both intraepithelial and stromal Ly6G⁺ cells in tumors from *Pten*^{pc/-}*Smad4*^{pc/-} mice and *Pten*^{pc/-} mice (Fig. 3E and F). It has been shown previously that ROS production by PMN-MDSCs is one of the mechanisms driving immune suppression (5, 14–16). Correspondingly, IPA revealed that pathways involved in ROS and nitric oxide (NO) production are among the top pathways activated in *Pten*^{pc/-}*Smad4*^{pc/-} tumors (Fig. 1A, arrow). Consistent with the increased infiltration of PMN-MDSCs in the *Pten*^{pc/-}*Smad4*^{pc/-} tumors, the expression of several subunits of NADPH oxidase (*Nox2*, *p40*^{phox}, and *p47*^{phox}), which are responsible for ROS production in PMN-MDSCs (5), was significantly upregulated in *Pten*^{pc/-}*Smad4*^{pc/-} tumors relative to *Pten*^{pc/-} tumors (Fig. 3G). Moreover, *Arg1*, but not *Nos2*, was highly upregulated in the *Pten*^{pc/-}*Smad4*^{pc/-} tumors (Fig. 3G). Together, MDSCs in autochthonous *Pten*^{pc/-}*Smad4*^{pc/-} tumors display strong T-cell-suppressive activity and are predominantly the PMN-MDSC subtype.

Immunodepletion of MDSCs Impedes Tumor Progression in *Pten*^{pc/-}*Smad4*^{pc/-} Mice

Enrichment of MDSCs in advanced *Pten*^{pc/-}*Smad4*^{pc/-} tumors prompted us to explore the possible role of MDSCs in tumor progression. Using a well-characterized anti-Gr1 neutralizing monoclonal antibody (clone RB6-8C5; ref. 17), MDSCs were depleted in *Pten*^{pc/-}*Smad4*^{pc/-} mice at 14 weeks of age, a point coincident with progression to the early invasive carcinoma stage (see Supplementary Fig. S3A for treatment scheme). The potent MDSC depletion activity of anti-Gr1 monoclonal antibody was evidenced by significantly decreased PMN-MDSCs and M-MDSCs in peripheral blood as early as day 2 after treatment (Supplementary Fig. S3B). In

Figure 1. Prominent infiltration of immune cells in the *Pten^{pc/-}Smad4^{pc/-}* tumors as compared with *Pten^{pc/-}* tumors. **A**, the top 10 activated pathways in *Pten^{pc/-}Smad4^{pc/-}* tumors ($n = 5$) as compared with *Pten^{pc/-}* tumors ($n = 5$) identified by IPA. RAR, retinoic acid receptor. **B**, a significant increase in the infiltration of immune cells as shown by IHC for CD45 in *Pten^{pc/-}Smad4^{pc/-}* tumors as compared with *Pten^{pc/-}* tumors from 16-week-old mice ($n = 3$). AP, anterior prostate; VP, ventral prostate; DLP, dorsolateral prostate; H&E, hematoxylin and eosin staining. Scale bars, 200 μ m. **C**, quantification of tumor-infiltrating CD45⁺ cells (AP, VP, and DLP combined) in *Pten^{pc/-}* tumors and *Pten^{pc/-}Smad4^{pc/-}* from 16-week-old mice ($n = 3$), assessed by CyTOF. **D**, percentages of various immune cell populations within the CD45⁺-infiltrating immune cells in prostate tumors from 16-week-old *Pten^{pc/-}* and *Pten^{pc/-}Smad4^{pc/-}* mice, assessed with CyTOF (9-marker) and analyzed with FlowJo. CD11b⁺ myeloid cells are significantly greater in *Pten^{pc/-}Smad4^{pc/-}* tumors as compared with *Pten^{pc/-}* tumors ($n = 3$; $P < 0.05$).



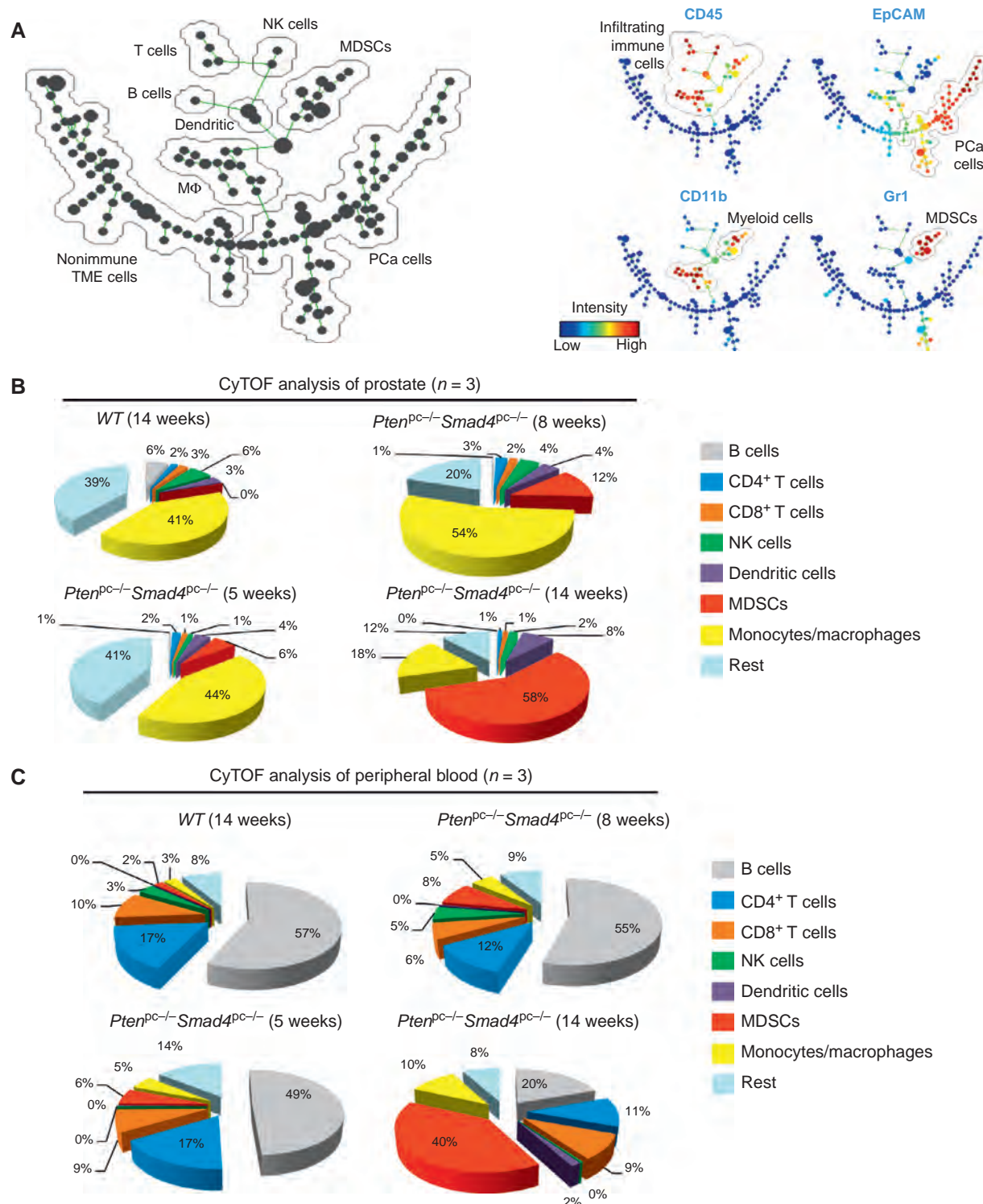


Figure 2. CD11b⁺Gr1⁺ cells are significantly increased in *Pten*^{pc/-}*Smad4*^{pc/-} tumors as compared with *Pten*^{pc/-} tumors. **A**, SPADE tree derived from CyTOF (17-marker) analysis of whole-tumor cell population from *Pten*^{pc/-}*Smad4*^{pc/-} mice at 5 weeks, 8 weeks, and 14 weeks of age (n = 3). Live single cells were used to construct the tree. Cell populations were identified as prostate cancer (PCa) cells (EpCAM⁺CD45⁺), nonimmune TME cells (EpCAM⁺CD45⁻), T cells (CD45⁺CD3⁺TCRβ⁺), B cells (CD45⁺B220⁺CD19⁺), natural killer (NK) cells (CD45⁺NK1.1⁺), dendritic cells (CD45⁺CD11c⁺), putative MDSCs (CD45⁺CD11b⁺Gr1⁺), and macrophages (CD45⁺CD11b⁺Gr1⁻). On the right plots, the tree is colored by the median intensity of individual markers shown on the top to highlight infiltrating immune cells (EpCAM⁺CD45⁺), epithelial prostate cancer cells (EpCAM⁺CD45⁻), total myeloid cells (CD45⁺CD11b⁺), and putative MDSCs (CD45⁺CD11b⁺Gr1⁺). **B** and **C**, CyTOF analysis of tumors (**B**) or peripheral blood (**C**) from 5-, 8-, and 14-week-old *Pten*^{pc/-}*Smad4*^{pc/-} mice revealed an age-dependent increase in the MDSC infiltration. Prostate from wild-type (WT) mice at 16 weeks old was used as control (n = 3 for each genotype). See also Supplementary Fig. S1.

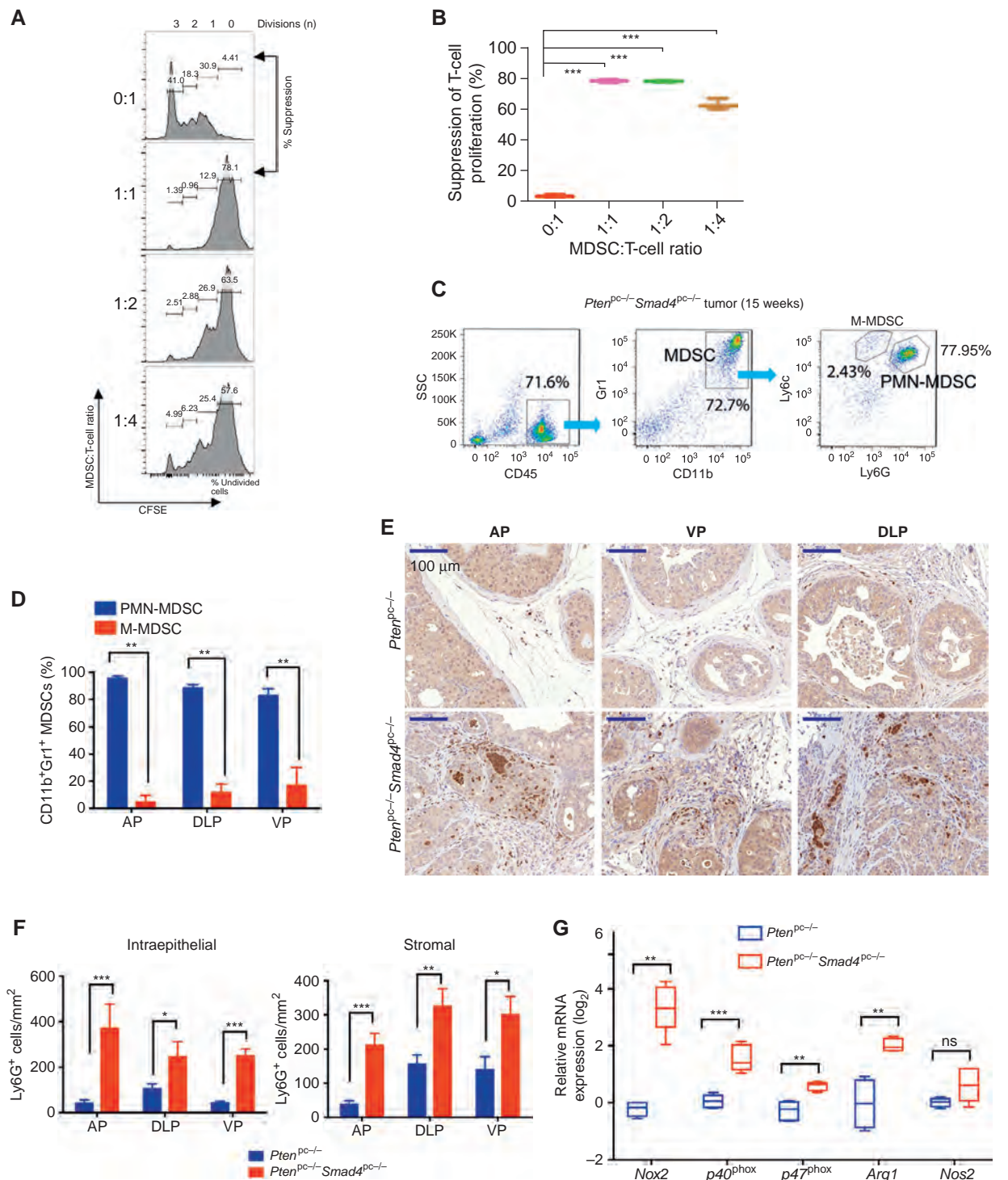


Figure 3. MDSCs from *Pten^{pc-/-}Smad4^{pc-/-}* tumors display potent immunosuppressive activities and are dominated by PMN-MDSCs. **A**, CD11b⁺Gr1⁺ cells from *Pten^{pc-/-}Smad4^{pc-/-}* tumors display potent immune-suppressive activity toward T-cell activation as demonstrated by CFSE dilution assay in triplicate. **B**, summarized result from **A**. **C** and **D**, flow cytometry analysis shows PMN-MDSCs as the major population in the infiltrated MDSCs in established *Pten^{pc-/-}Smad4^{pc-/-}* tumors at AP, DLP, and VP ($n = 5$). SSC, side scatter. **E** and **F**, a significant increase in Ly6G⁺ cells in *Pten^{pc-/-}Smad4^{pc-/-}* tumors as compared with the *Pten^{pc-/-}* tumors as shown by IHC for Ly6G and quantified by location of positively stained cells in the intraepithelial or stromal compartment of the tumor at AP, DLP, and VP ($n = 3$). **G**, quantification of the mRNA expression of subunits of NADPH oxidase (*Nox2*, *p40^{phox}*, and *p47^{phox}*), *Arg1*, and *Nos2* in the *Pten^{pc-/-}Smad4^{pc-/-}* tumors and the *Pten^{pc-/-}* tumors ($n = 5$). In **B**, **D**, **F**, and **G**, *, $P < 0.05$; **, $P < 0.01$; ***, $P < 0.001$; ns, nonsignificant. Also see Supplementary Fig. S2.

addition, a systemic reduction of MDSCs in spleen, bone marrow, and prostate tumors was documented following a 30-day treatment regimen of anti-Gr1 monoclonal antibody (Fig. 4A and Supplementary Fig. S3C). This MDSC depletion was accompanied by an increase of CD8⁺ T cells (so-called killer T cells; Fig. 4A), consistent with elimination of the T-cell suppression activity of MDSCs. Importantly, in line with the CD8⁺ T-cell expansion, we observed that the Gr1-treated prostate displayed remarkable weight reduction in ventral and dorsolateral prostates (VP and DLP; Fig. 4B). The lack of difference in the weight of the anterior prostate (AP) is likely due to the fact that the AP tends to develop cysts with fluid accumulated inside the gland (18, 19), which also prevents the accurate measure of the prostate weight (Supplementary Fig. S3D). Histopathologic analysis revealed adenocarcinoma was the predominant pathology in mice treated with the control IgG, whereas mouse prostatic intraepithelial neoplasia (mPIN) was the predominant morphologic presentation in prostates from mice treated with anti-Gr1 monoclonal antibody (Fig. 4C and Supplementary Table S2). In addition, by immunohistochemical staining for CD45, Ki67, vimentin, smooth muscle actin (SMA), and Trichrome staining, we observed that tumor remnants in mice treated with anti-Gr1 monoclonal antibody displayed markedly reduced levels of cellular proliferation, stromal reaction, and inflammation as compared with those tumors treated with control IgG antibody (Supplementary Fig. S4A).

In another therapeutic trial, we also utilized the recently developed MDSC-specific peptide-Fc fusion protein (i.e., peptibodies) that has been shown to effectively eliminate MDSCs *in vivo* through targeting the S100A9 surface protein (20). Employing a hydrodynamic injection approach for nucleic acid delivery (21), intravenous injection of either Pep-H6 peptibody expression vector or irrelevant control peptibody vector was initiated at 14 weeks every 4 days in *Pten*^{pc/-}/*Smad4*^{pc/-} mice. Strikingly, a single injection of the Pep-H6 peptibody significantly reduced the MDSCs in the peripheral blood, whereas such effect was not observed using the irrelevant control peptibody (Supplementary Fig. S4B). Pep-H6 peptibody treatment for 1 month led to a dramatic decrease in cancer cell content in the prostate tumors (Fig. 4D) and provided significant survival benefit for tumor-bearing mice (Fig. 4E). Together, our data strongly support the view that MDSC depletion blocks prostate tumor progression in the *Pten*^{pc/-}/*Smad4*^{pc/-} model.

CXCL5–CXCR2 Signaling Promotes MDSC Recruitment and CXCR2 Inhibition Delays Tumor Progression in *Pten*^{pc/-}/*Smad4*^{pc/-} Mice

To elucidate the cellular origins and signaling molecules governing MDSC recruitment to prostate tumors, we incorporated the *mTmG* dual fluorescence reporter allele into the *Pten*^{pc/-}/*Smad4*^{pc/-} model where signaling events between tumor cells and stroma can be precisely delineated. The *mTmG* allele (22) allows Cre-dependent GFP expression in prostate epithelial cells and ubiquitous tdTomato expression in all other non-Cre-expressing cells (Fig. 5A). Transcriptomic and IPA analyses of FACS-sorted GFP⁺ tumor cells and Tomato⁺ stromal cells showed distinct expression patterns by hierarchical clustering (Fig. 5A) with tumor cells enriched for pathways involved in cell adhesion molecules and tight junctions (consistent with

their epithelial nature) and stromal cells displaying activation of more diverse pathways involved in chronic inflammation, such as cytokine/cytokine receptor interaction, chemokine, JAK–STAT, T-cell receptor, and B-cell receptor signaling ($P < 0.01$, data not shown). This result is consistent with the immunopathologic and histopathologic analyses showing a massive infiltration of immune cells in the *Pten*^{pc/-}/*Smad4*^{pc/-} tumors.

Employing this new model, we sought to identify genes that were upregulated in *Pten*^{pc/-}/*Smad4*^{pc/-} cancer cells relative to *Pten*^{pc/-} cancer cells that might illuminate mechanisms involved in the recruitment of MDSCs by classifying the upregulated genes into either stroma- or tumor-enriched genes. To this end, our previously generated list of 242 genes with greater than 2-fold increased expression in *Pten*^{pc/-}/*Smad4*^{pc/-} relative to *Pten*^{pc/-} tumors (11) was intersected with 486 genes preferentially expressed in *Pten*^{pc/-}/*Smad4*^{pc/-} GFP⁺ cancer cells relative to Tomato⁺ stroma cells (fold change ≥ 4 ; Supplementary Tables S3 and S4), yielding 28 genes that are markedly enriched in *Pten*^{pc/-}/*Smad4*^{pc/-} cancer cells (Supplementary Table S5). Among these 28 genes, *Cxcl5*, which encodes a key cytokine involved in MDSC recruitment (23, 24), is the most significantly upregulated cancer cell-specific cytokine in *Pten*^{pc/-}/*Smad4*^{pc/-} tumors as compared with *Pten*^{pc/-} tumors (Fig. 5B and Supplementary Fig. S5A). Notably, CXCR2, the cognate receptor for CXCL5, is also upregulated in *Pten*^{pc/-}/*Smad4*^{pc/-} tumors as compared with *Pten*^{pc/-} tumors and is significantly enriched in *Pten*^{pc/-}/*Smad4*^{pc/-} Tomato⁺ stroma cells (Fig. 5B). The upregulation of CXCL5 expression in *Pten*^{pc/-}/*Smad4*^{pc/-} prostate tumors was further confirmed by IHC (Fig. 5C). In addition, we performed FACS analysis of CD11b⁺Gr1⁺ cells and CD11b⁺Gr1[−] cells from bone marrow, spleen, peripheral blood, and tumors for CXCR2 expression. As shown in Supplementary Fig. S5B, CD11b⁺Gr1[−] cells (largely lymphocytes) are devoid of CXCR2 expression, whereas a large fraction of CD11b⁺Gr1⁺ cells express CXCR2. When CXCR2 expression was further separated into CXCR2^{hi} and CXCR2⁺, we observed an enrichment of the CXCR2^{hi} subpopulation in the CD11b⁺Gr1⁺ cells in prostate tumors compared with CD11b⁺Gr1⁺ cells from bone marrow, spleen, or blood (Supplementary Fig. S5B). This is consistent with the model of active recruitment of MDSCs by tumors through CXCR2-mediated chemoattraction.

To validate the CXCL5–CXCR2 axis in the recruitment of MDSCs to the TME of *Pten*^{pc/-}/*Smad4*^{pc/-} tumors, we assessed the impact of pharmacologic inhibition of CXCL5 and CXCR2 in MDSCs using a transwell migration assay (23). First, anti-CXCL5-neutralizing antibody pretreatment of conditioned medium (CM) derived from *Pten*^{pc/-}/*Smad4*^{pc/-} prostate cancer cell line resulted in decreased migration of MDSCs (Fig. 5D). Second, CXCR2 inhibitor SB255002 or anti-CXCR2 neutralizing antibody pretreatment also impeded migration of MDSCs (Fig. 5D). Third, *in vivo* blockade of the CXCL5–CXCR2 axis using SB255002 in 14-week-old *Pten*^{pc/-}/*Smad4*^{pc/-} mice over a 14-day daily dosing schedule revealed a dramatic reduction in infiltration of MDSCs in the prostate tumors (Supplementary Fig. S5C and S5D). Notably, similar to mice treated with anti-Gr1 neutralizing antibody, these SB255002-treated *Pten*^{pc/-}/*Smad4*^{pc/-} mice also showed significant reduction in tumor burden (VP and DLP) as compared with the vehicle-treated controls (Fig. 5E and Supplementary Fig. S5E). Strikingly,

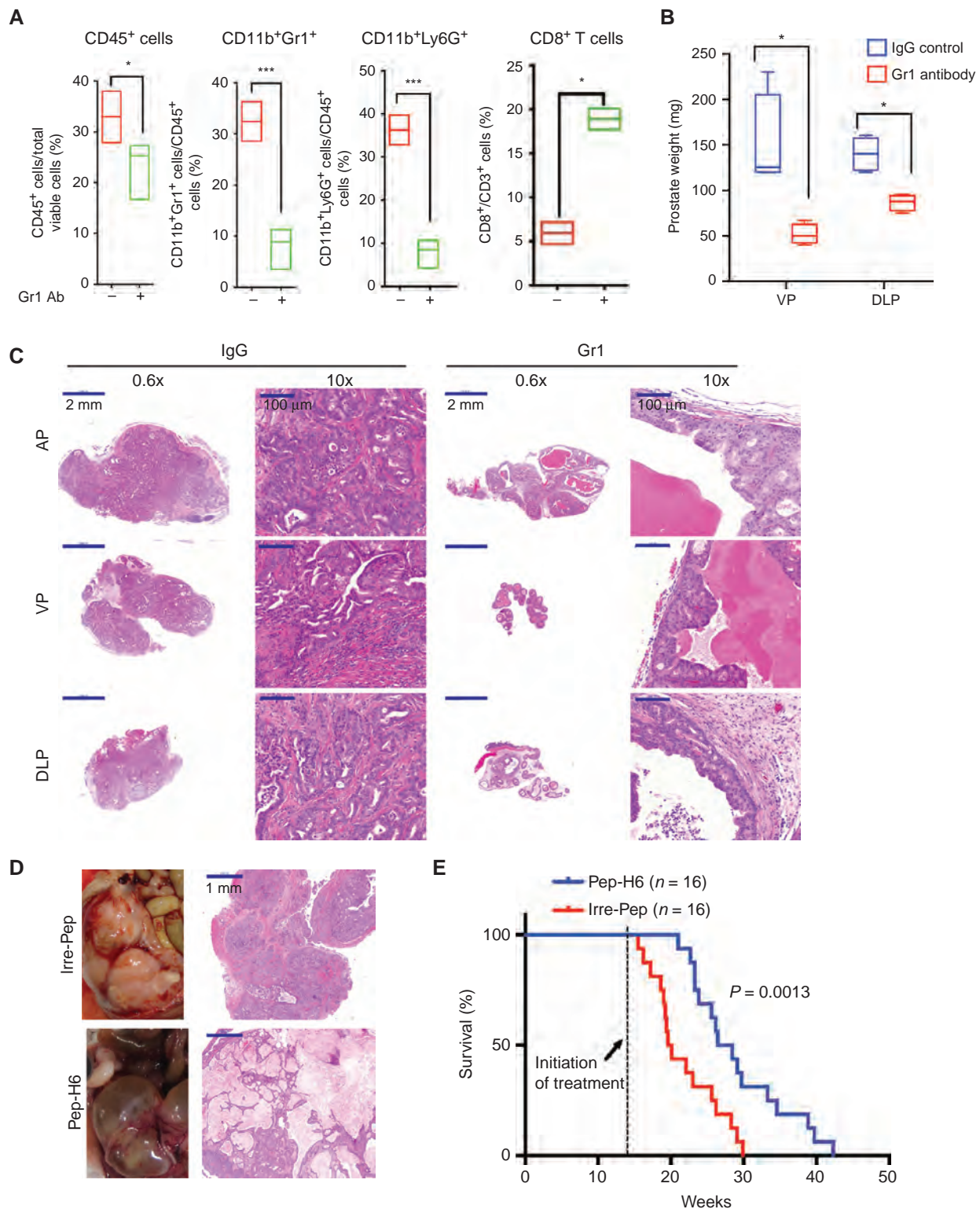


Figure 4. Targeting MDSCs with anti-Gr1 neutralizing antibody or MDSC-specific peptibody significantly delayed tumor progression in *Pten^{pc/-}Smad4^{pc/-}* mice. **A**, administration of Gr1-neutralizing antibody *in vivo* significantly reduced CD45⁺-infiltrating immune cells, reduced MDSCs, and increased CD8⁺ T cells among total T cells in *Pten^{pc/-}Smad4^{pc/-}* tumors (n = 4), measured by flow cytometry. **B**, Gr1 antibody treatment of 14-week-old mice significantly reduced the weight of VP and DLP in *Pten^{pc/-}Smad4^{pc/-}* mice. **C**, Gr1 antibody treatment remarkably altered the tumor histopathology in *Pten^{pc/-}Smad4^{pc/-}* adenocarcinoma, analyzed by hematoxylin and eosin staining of AP, VP, and DLP. **D**, one month of Pep-H6 peptibody treatment led to significant appearance and histology changes of the *Pten^{pc/-}Smad4^{pc/-}* adenocarcinoma. Irre-Pep, irrelevant control peptibody. **E**, Kaplan-Meier survival curve showing the significant delay of mortality caused by Pep-H6 peptibody treatment of *Pten^{pc/-}Smad4^{pc/-}* mice. In **A** and **B**, *, *P* < 0.05 and ***, *P* < 0.001; Also see Supplementary Figs. S3 and S4.

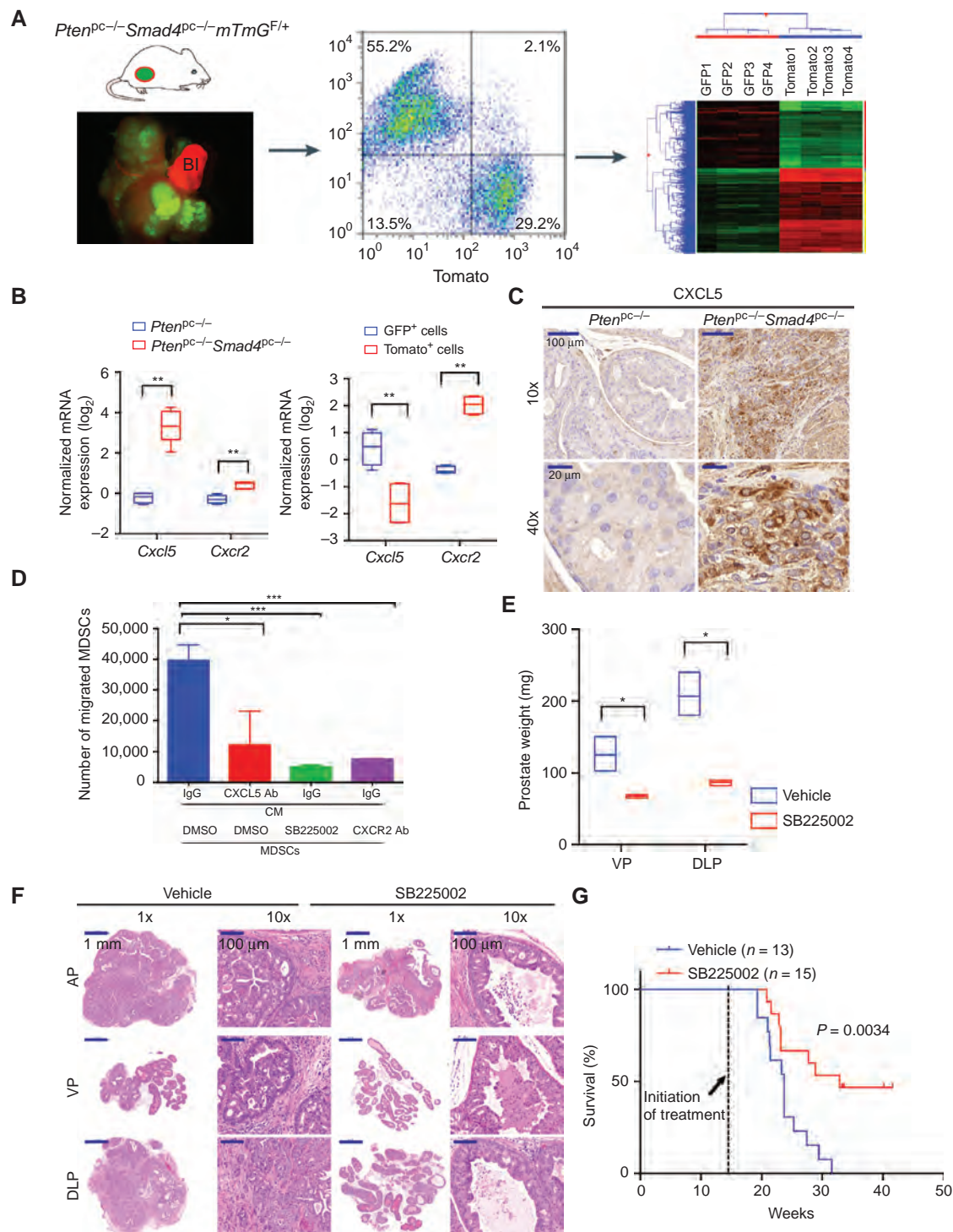


Figure 5. CXCL5-CXCR2 axis plays an indispensable role in recruitment of MDSCs and promotion of tumor progression. **A**, establishment of *Pten^{pc-/}Smad4^{pc-/}mTmG^{F/+}* model allows fluorescent visualization of the GFP⁺ tumor cells intermixed with Tomato⁺ stroma (left); FACS isolation of GFP⁺ tumor cells and Tomato⁺ stromal cells from the prostate adenocarcinoma (middle); microarray analysis to identify differentially expressed genes (right). In the fluorescence image, Bl denotes bladder (completely Tomato⁺; n = 2). **B**, quantification of mRNA expression shows that *Cxcl5* and *Cxcr2* were both expressed at higher levels in *Pten^{pc-/}Smad4^{pc-/}* tumors than in *Pten^{pc-/}* tumors, and *Cxcl5* expression was enriched in GFP⁺ tumor cells, whereas *Cxcr2* expression was enriched in Tomato⁺ stromal cells (n = 5). **C**, IHC for CXCL5 showed significantly higher expression levels of CXCL5 in *Pten^{pc-/}Smad4^{pc-/}* tumors than *Pten^{pc-/}* tumors (n = 3). **D**, blocking the CXCL5-CXCR2 axis by CXCL5-neutralizing antibody, CXCR2 inhibitor SB225002, or CXCR2-neutralizing antibody significantly decreased migration of MDSCs toward conditioned medium from *Pten^{pc-/}Smad4^{pc-/}* tumor cells, evaluated with an *in vitro* transwell migration assay in triplicate. **E** and **F**, CXCR2 inhibitor SB225002 treatment of *Pten^{pc-/}Smad4^{pc-/}* mice for 14 days (n = 4) resulted in significantly reduced tumor weight of VP and DLP and significantly delayed progression for AP prostate cancer shown by hematoxylin and eosin staining. **G**, CXCR2 inhibitor SB225002 treatment of *Pten^{pc-/}Smad4^{pc-/}* mice significantly prolonged their overall survival. In **B**, **D**, and **E**, *, P < 0.05; **, P < 0.01; and ***, P < 0.001. Also see Supplementary Fig. S5.

all SB225002-treated tumors presented with prostatic intraepithelial neoplasia (PIN) pathology, whereas the control group uniformly possessed advanced adenocarcinoma (Fig. 5F and Supplementary Table S2). Furthermore, SB225002 treatment significantly prolonged the overall survival of the *Pten*^{PC/-}*Smad4*^{PC/-} mice as compared with the vehicle control (Fig. 5G). Thus, we conclude that the CXCL5–CXCR2 axis plays a prominent role in the recruitment of MDSCs to the *Pten*^{PC/-}*Smad4*^{PC/-} prostate TME and that inhibition of this axis profoundly impairs tumor progression.

YAP1 Is Activated in *Pten*^{PC/-}*Smad4*^{PC/-} Tumors and Directly Regulates *Cxcl5* Transcription

Having identified cancer cell–derived CXCL5 as a key signaling molecule governing recruitment of MDSCs into the TME, we sought to define the molecular mechanisms underlying the strong induction of CXCL5 expression in the *Pten*^{PC/-}*Smad4*^{PC/-} cancer cells. As CXCL5 expression is not significantly upregulated in the *Pten*^{PC/-} tumors (Fig. 5C), we performed unbiased Gene Set Enrichment Analysis (GSEA) to identify pathways that were activated in the *Pten*^{PC/-}*Smad4*^{PC/-} tumors as compared with *Pten*^{PC/-} tumors, aiming to identify potential regulators for *Cxcl5* in *Pten*^{PC/-}*Smad4*^{PC/-} tumors. The YAP oncogenic signature emerged as the second most hyperactivated pathway (Fig. 6A and Supplementary Fig. S6A). Although it is known that the Hippo–YAP pathway plays an important role in development and cancer in organs such as the liver, skin, intestine, and pancreas (25–27), the role for the Hippo–YAP pathway in prostate cancer biology is emerging. Specifically, Hippo pathway components LATS1/2 have been implicated in anoikis and metastasis in prostate cancer (28), and ERG-induced YAP1 activation can promote age-related prostate tumor development (29). However, beyond the cancer cell–specific functions, the Hippo–YAP1 pathway has not been linked to signaling communication between cancer cells and immune cells in the TME. Consistent with the *in silico* analysis, IHC analysis documented a dramatic increase in the nuclear localization of YAP1 in *Pten*^{PC/-}*Smad4*^{PC/-} cancer cells as compared with *Pten*^{PC/-} cancer cells (Fig. 6B). As YAP1, a transcriptional coactivator and the downstream mediator of Hippo signaling, is regulated posttranscriptionally by either kinase-mediated degradation or cytoplasmic sequestration (25), our findings of increased nuclear localization of YAP1 are consistent with the hypothesis that the Hippo–YAP pathway is activated in the *Pten*^{PC/-}*Smad4*^{PC/-} tumors. In addition, unbiased oPOSSUM analysis (30) indicated that TEAD1, a member of the TEAD transcription factor family that is required for YAP1 function, ranked second among the top 10 transcription factors with over-represented binding sites in the 70 cancer-specific genes that were upregulated in the *Pten*^{PC/-}*Smad4*^{PC/-} tumors as compared with the *Pten*^{PC/-} tumors (≥ 1.5 fold, Z-Score = 13.362; Supplementary Fig. S6B and S6C), an observation reinforcing the relevance of the Hippo–YAP pathway. Furthermore, we identified six YAP/TEAD binding motifs in the promoter of *Cxcl5* gene (Supplementary Fig. S6D), suggesting YAP1 could be directly involved in the recruitment of MDSCs through regulating *Cxcl5* expression. This hypothesis was supported by chromatin immunoprecipitation (ChIP) assay showing that YAP1 binds to *Cxcl5* promoter (Fig. 6C) and that shRNA-mediated knockdown of *Yap1* in *Pten*^{PC/-}*Smad4*^{PC/-} cancer cells drastically reduced the expression of *Cxcl5* mRNA (Fig. 6D). In addition, overexpression of a constitutively active

YAP1^{S127A} mutant dramatically increased *Cxcl5* mRNA expression in the *Pten*^{PC/-}*Smad4*^{PC/-} cell line (Fig. 6E), whereas overexpression of a TEAD binding defective YAP1 mutant S127A/S94A compromised its ability to activate *Cxcl5* transcription (Fig. 6F). To examine the effect of YAP1-dependent cytokine signaling in the regulation of MDSCs recruitment, we first prepared CM from the *Pten*^{PC/-}*Smad4*^{PC/-} cell line either infected with shRNA against *Yap1* or pretreated with verteporfin (25), a small-molecular inhibitor that disrupts YAP1–TEAD interaction. We then tested the effect of various CM on the migration of MDSCs *in vitro*. As shown in Fig. 6G and H, we observed significantly decreased MDSC migration *in vitro* when CM was from cells with either YAP1 knockdown or verteporfin treatment.

Finally, to test if targeting YAP1 *in vivo* can impair the infiltration of MDSCs and inhibit tumor growth, we used our recently isolated syngeneic murine prostate cancer line PPS, which is derived from the backcrossed *Pten*^{PC/-}*Smad4*^{PC/-}*Trp53*^{PC/-} model (31) and can form subcutaneous or orthotopic tumors robustly in C57BL/6 hosts. Doxycycline-dependent shRNA knockdown of *Yap1* (two independent shRNA designs #1 and #3) was established in PPS (Fig. 6I) and injected subcutaneously in C57BL/6 mice. YAP1 knockdown induced by switching to doxycycline-containing drinking water resulted in a reduction of MDSCs in the intratumoral CD45⁺ population (Fig. 6J and K) and impaired tumor progression (Fig. 6L). Although the observation supports the hypothesis that targeting YAP1-dependent MDSC infiltration impairs tumor growth, we acknowledge that the tumor growth impediment by YAP1 silencing is likely due to a combined effect of both cell-nonautonomous and cell-autonomous mechanisms. Together, these findings reveal a novel function for YAP1 in the recruitment of MDSCs through direct upregulation of *Cxcl5* transcription in prostate tumor cells.

YAP1 Is Activated in Human Prostate Cancer and Tracks with an MDSC Signature

To determine whether YAP1 is overexpressed and activated in human prostate cancer, we performed IHC staining of a human prostate cancer tissue microarray (TMA) for YAP1. Interestingly, YAP1 is expressed in basal cells, but not in the luminal cells of the normal human prostate (Fig. 7A). In addition, we observed that YAP1 is overexpressed in a subset of human prostate cancers (Fig. 7A and B and Supplementary Table S6), consistent with a recent report (29). Given the lack of validated antibodies for human MDSCs for TMA analysis, we generated a list of 39 MDSC-related genes curated from literature analysis (Supplementary Table S7) to generate evidence of a link between YAP1 activation and MDSC prominence in human prostate. Using the prostate RNA-sequencing data from The Cancer Genome Atlas (TCGA), unsupervised clustering with the 39-gene MDSC signature categorized 498 TCGA primary prostate tumors into three subtypes: MDSC-high ($n = 139$), MDSC-medium ($n = 158$), and MDSC-low ($n = 201$; Fig. 7C), suggesting that a subset of human prostate tumors may have prominent infiltration of MDSCs. In addition, using GSEA, we found that several YAP1 signature genes are significantly overexpressed in MDSC-high samples as compared with MDSC-low samples (Fig. 7D; P value < 0.005), reinforcing the link between MDSC-high prostate tumors and YAP1 transcriptional activities. Furthermore,

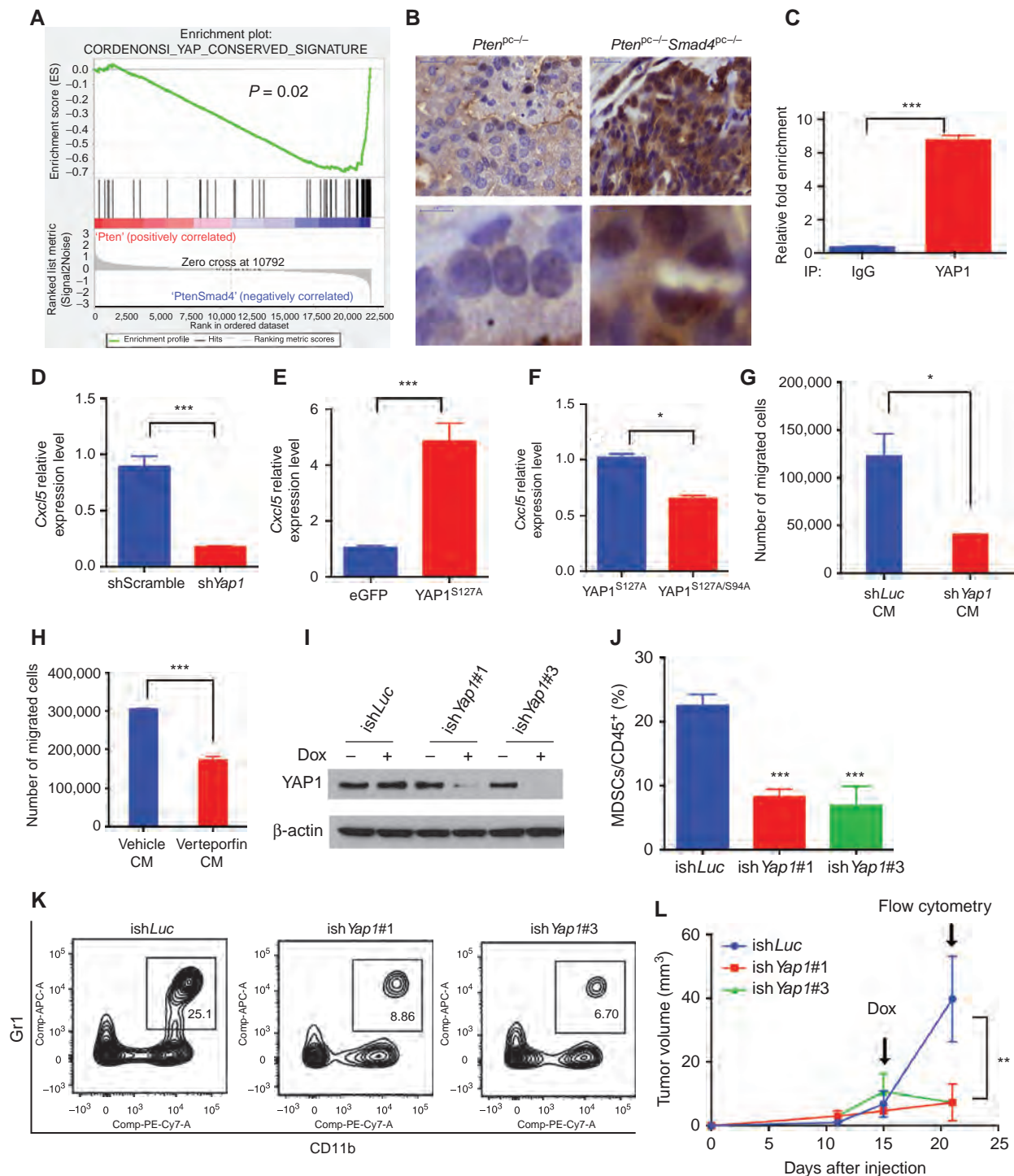


Figure 6. Hyperactivation of YAP1 in *Pten^{pc-/}Smad4^{pc-/}* tumors upregulates *Cxcl5*. **A**, GSEA analysis identified the YAP1 oncogenic signature as the top activated pathway in the *Pten^{pc-/}Smad4^{pc-/}* tumors compared with *Pten^{pc-/}* tumors ($n = 5$). **B**, a significant increase in nuclear staining for YAP1 in the *Pten^{pc-/}Smad4^{pc-/}* tumors compared with *Pten^{pc-/}* tumors ($n = 3$). **C**, ChIP shows that YAP1 can directly bind to *Cxcl5* promoter using quantitative PCR in triplicates. **D**, shRNA knockdown of *Yap1* in *Pten^{pc-/}Smad4^{pc-/}* tumor cells resulted in a dramatic reduction in *Cxcl5* mRNA expression using quantitative PCR in triplicate. **E**, overexpression of a constitutively active YAP1^{S127A} mutant resulted in upregulation of *Cxcl5* mRNA using quantitative PCR in triplicate. **F**, TEAD-binding defective YAP1^{S127A/S94A} mutant significantly decreased *Cxcl5* mRNA expression as compared with the YAP1^{S127A} mutant using quantitative PCR in triplicate. **G** and **H**, conditioned medium prepared from *Pten^{pc-/}Smad4^{pc-/}* cells infected with *Yap1* shRNA (**G**) or treated with verteporfin (**H**), a small molecule that disrupts YAP1-TEAD interaction, induced less MDSC migration *in vitro* as compared with the control conditioned medium. Transwell migration was done in triplicate for each condition. **I**, Western blot analysis showed that two independent inducible shRNAs for *Yap1* efficiently knock down *Yap1* expression in the *Pten^{pc-/}Smad4^{pc-/}* cells. **J–L**, inducible *Yap1* knockdown strongly suppressed the intratumoral MDSC infiltration (**J** and **K**) and tumor growth (**L**) of the C57BL/6-syngeneic cell line isolated from prostate tumor of *Pten^{pc-/}Smad4^{pc-/}Trp53^{pc-/}* mice ($n = 5$). In **C**, **D**, **E** and **F**, **G**, **H**, **L**, *, $P < 0.05$; **, $P < 0.01$; ***, $P < 0.001$. See also Supplementary Fig. S6.

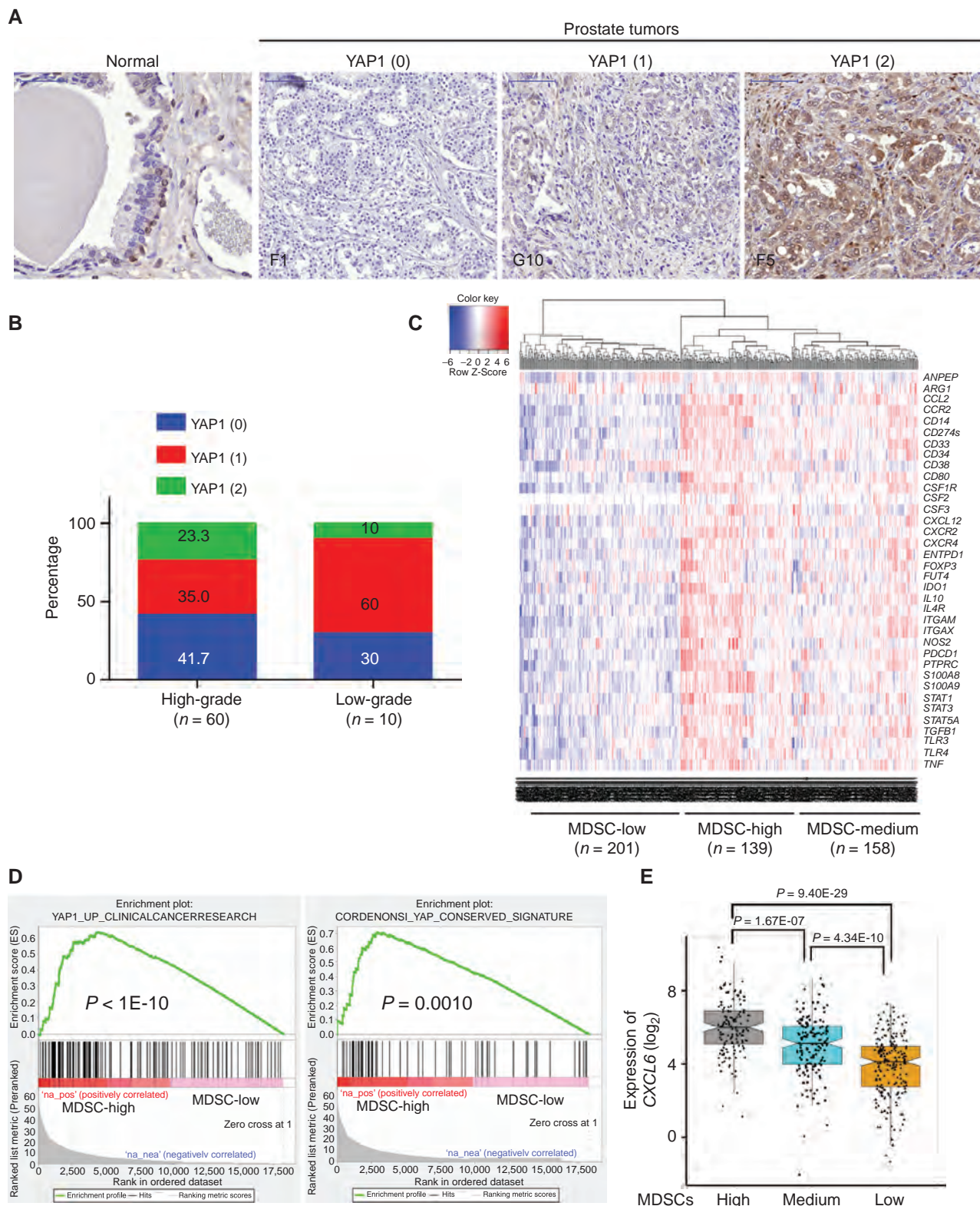


Figure 7. YAP1 is activated in human prostate cancer and correlated with MDSC signature and CXCL6 overexpression. **A**, IHC analysis of YAP1 expression in basal cells of normal prostate tissue and human prostate cancers. Numbers in parentheses indicate YAP1 IHC intensity scores. **B**, YAP1 IHC intensity score representation in low-grade (n = 10) and high-grade (n = 60) prostate cancer. **C**, clustering of human TCGA prostate samples into MDSC-high, MDSC-low, and MDSC-medium groups using a 39-gene MDSC signature. **D**, YAP1 signatures are identified in MDSC-high prostate TCGA samples. **E**, CXCL6 expression is significantly higher in the MDSC-high group. See also Supplementary Fig. S7.

CXCL6, the human homolog of murine *Cxcl5*, is expressed at higher levels in the MDSC-high samples as compared with MDSC-low samples (Fig. 7E; $P = 9.40E-29$). Similar analysis was performed in a published dataset focused on tumor immunobiological differences in prostate cancer between African-American and European-American men (32). The 39-gene MDSC signature can cluster the 69 primary prostate tumors into MDSC-high ($n = 40$) and MDSC-low groups ($n = 29$), and YAP1 signatures were prominent in the MDSC-high groups (Supplementary Fig. S7A and S7B). Together, these human prostate tumor findings, which parallel our murine observations, suggest that activated YAP1 is integral to MDSC infiltration in both mouse and human prostate cancer, thus enhancing the translational value of the study.

DISCUSSION

Although a large number of studies have demonstrated a direct relationship between MDSC frequency and tumor burden (5), our understanding of the role of MDSCs in tumor progression, particularly prostate cancer, remains largely speculative. Here, using a highly invasive PTEN/SMAD4-deficient prostate cancer model, we established the signaling circuits involved in the recruitment of MDSCs to the TME and demonstrated a critical role of these cells in facilitating tumor progression.

Homozygous deletion of *Pten* in murine prostate elicited a strong senescence response that restricts tumor progression (33); thus, *Pten*-deficient prostate tumors are largely indolent and progress slowly to invasive prostate adenocarcinoma without metastasis to distant organs (11, 33). Recently, it was shown that infiltrating Gr1⁺ myeloid cells suppress *Pten* loss-induced cellular senescence through a paracrine signaling mediated by myeloid-secreted IL1RA (10). We have previously reported that deletion of *Smad4* leads to bypass of *Pten* loss-induced senescence in prostate cancer progression, resulting in aggressive cancer cell proliferation and invasion/metastasis (11). Using the state-of-the-art CyTOF technology, we revealed that progression in the *Pten*^{pc/-}*Smad4*^{pc/-} model is associated with abundant immune cell infiltration characterized by prominent representation of CD11b⁺Gr1⁺ MDSCs, which display potent immunosuppressive activities as shown by their strong antagonistic effect on T-cell proliferation (Fig. 3A and B).

The basis for the increased frequency of MDSCs in the TME and, specifically in the *Pten*^{pc/-}*Smad4*^{pc/-} model, was not known and presumably could derive from either active chemoattraction or passive nonspecific responses to tissue stress associated with expanding tumor burden. Taking an unbiased approach to identify pathways that may recruit MDSCs, we deconvoluted cancer versus stromal cell transcriptomes by exploiting a Cre-dependent dual fluorescence lineage tracing system in the *Pten*^{pc/-}*Smad4*^{pc/-} model. This approach identified unique immune regulatory molecules that are activated prominently in *Pten*^{pc/-}*Smad4*^{pc/-} cancer cells, most prominently CXCL5. We established that the CXCL5 chemokine plays a key role in the efficient recruitment of MDSCs which enables tumor progression, as blocking CXCL5–CXCR2 signaling with a CXCR2 inhibitor led to reduced MDSC infiltration with associated antitumor effects. It should be noted that the human homolog for murine CXCL5 is CXCL6, and CXCL6 has been shown to be upregulated in prostate cancer as compared with normal

prostate and significantly associated with high Gleason scores 8 to 9 (34). Interestingly, it was shown that CXCL5 promotes recruitment of MDSCs to primary melanoma, resulting in epithelial-mesenchymal transition (EMT) and cancer cell dissemination (35). Thus, the possible role of CXCL5/CXCL6 in prostate cancer metastasis merits further study.

Our finding that CXCL5 is the main chemoattractant in the *Pten*^{pc/-}*Smad4*^{pc/-} model also provided a framework to determine the cancer cell signaling pathways driving *Cxcl5* upregulation. By integration of bioinformatic analysis and experimental validation, we identified that YAP1 is activated in *Pten*^{pc/-}*Smad4*^{pc/-} prostate tumors and that YAP1 directly regulates *Cxcl5* transcription and MDSC recruitment. In addition, we showed that YAP1 is overexpressed in a subset of human prostate cancers, which is consistent with a recent publication showing a correlation of ERG and YAP1 coexpressed in a subset of human prostate cancers (29). Importantly, a 39-gene MDSC signature clusters the prostate TCGA samples into three subtypes. By comparing the samples with high and low abundance of MDSC-related gene expression, YAP1 signatures and higher expression of CXCL6 are identified in the MDSC-high samples, which is consistent with our findings in the mouse model. Furthermore, the 39-gene MDSC signature can cluster primary prostate tumor samples from a published dataset (32) into two subtypes using MDSC-high and MDSC-low, with YAP1 signatures identified in the MDSC-high subtype. The Hippo–YAP signaling pathway is widely deregulated in human solid neoplasia and often associated with enhanced cancer cell proliferation and cancer stem cell phenotypes (25), and is implicated in the regulation of anoikis and metastasis in prostate cancer (28) and the development of age-related prostate cancers driven by ERG overexpression (29), yet how the Hippo–YAP pathway regulates the TME in prostate cancer has hitherto not yet been elucidated. Our finding of a novel non-cell autonomous function for Hippo–YAP signaling in MDSC recruitment in TME complements well the recently elucidated roles of YAP1 in promoting cell-autonomous functionality of cancer cells, including enhanced tumor survival, EMT, and bypass mechanism for oncogene addiction (26, 27).

Pharmacologic depletion of MDSCs using Gr1 antibody, Pep-H6 peptibody, or CXCR2 inhibitor arrested prostate progression at the high-grade PIN stage whereas controls exhibited full-fledged adenocarcinoma in *Pten*^{pc/-}*Smad4*^{pc/-} model. Given that treatment commences at 14 weeks of age (Supplementary Fig. S3A), when prostate tumors have uniformly advanced to the invasive adenocarcinoma stage (11) with significant MDSC infiltration (Fig. 2B), our findings support the view that anti-MDSC treatment provokes regression of advanced tumors. In addition, both Pep-H6 peptibody and CXCR2 inhibitor treatment significantly prolonged the overall survival of the *Pten*^{pc/-}*Smad4*^{pc/-} tumor-bearing mice. Therefore, our preclinical data suggest that pharmacologic depletion of MDSCs may offer potential therapeutic benefits for patients with advanced prostate cancer, particularly those deficient for PTEN and SMAD4. In line with our findings, others have demonstrated that depletion of G-MDSCs promotes the intratumoral accumulation of activated CD8⁺ T cells and apoptosis of tumor epithelial cells in a *Kras*/*Trp53* mouse pancreatic cancer model (36).

MDSCs are of myeloid cell lineage, and their coordinated regulation represents one of the most complex aspects of cancer–host interactions (37). The involvement of the myeloid compartment of the hematopoietic system in innate immunity, adaptive immunity, as well as in regulation of TME through nonimmune mechanisms highlights the need to understand more deeply how modulating different myeloid populations, including MDSCs, can positively or negatively affect tumor growth.

Pep-H6 peptibody, targeting S100A9 expressed on MDSCs, has been shown to have minimal toxicity in treated mice (20) and potent antitumor activity (Fig. 4D and E; ref. 18). Interestingly, tasquinimod, a small-molecular inhibitor for S100A9, has been shown to increase progression-free survival and overall survival for metastatic castration-resistant prostate cancer in a phase II clinical trial and has entered phase III clinical trials (38). Importantly, similar to the peptibody treatment in mice, tasquinimod is well tolerated and causes only minor adverse effects in human patients (38), suggesting that tasquinimod or similar drugs targeting S100A9 could potentially be used as chemopreventive agents for patients with high-risk primary prostate cancer. The antiproliferative mechanism may explain why targeting CXCR2 in prostate cancer with abundant preexisting MDSC infiltration can lead to MDSC depletion, as MDSCs have been shown to undergo active proliferation inside the prostate tumor of the *Pten*^{pc/-} model (9). The effectiveness of targeting CXCR2 in our model suggests targeting mechanisms that specifically regulate MDSC recruitment as well as their proliferative and survival potential in human cancers would provide therapeutic benefit for patients with prostate cancer.

Targeting MDSCs as a cooperative approach for immunotherapy is clinically relevant, as increasing evidence indicates MDSCs represent a *bona fide* immunosuppressive cell population in patients with various solid tumors (39, 40). Immunosuppressive mechanisms by MDSCs in mice have been validated in humans, which include L-arginine depletion, NO and ROS production, TGF β secretion, blocking T_{eff} cells and inducing T_{reg} cells, among others (39). Future studies are warranted to evaluate if combining MDSC depletion with immune checkpoint inhibitors, such as anti-CTLA-4, anti-PD-1, and anti-PD-L1 antibodies, may elicit synergistic efficacy in preclinical models of prostate cancer and eventually benefit patients with prostate cancer.

METHODS

Mice Strains

Pten^{pc/-} and *Pten*^{pc/-}*Smad4*^{pc/-} models were developed previously (11) and were backcrossed to the C57BL/6 background for more than four generations. B6.129(Cg)-Gt(ROSA)26Sortm4(ACTB-tdTomato,EGFP)Luo/J (“mTmG”) strain was obtained from The Jackson Laboratory. Mice were maintained in pathogen-free conditions at the MD Anderson Cancer Center. All manipulations were approved under the MD Anderson Cancer Center Institutional Animal Care and Use Committee.

Cell Lines

Pten^{pc/-}*Smad4*^{pc/-} prostate cell lines, which have been described previously (11), were generated in 2010. PPS, a C57BL/6-syngeneic cell line isolated from prostate tumors of *Pten*^{pc/-}*Smad4*^{pc/-}*Trp53*^{pc/-} mice, was generated in 2013. All cell lines tested for *Mycoplasma* were

negative within 6 months of performing the experiments. Cell line authentication was not performed.

CyTOF and Flow Cytometry

Prostate tumor single cells were isolated using the Mouse Tumor Dissociation Kit (Miltenyi Biotec). Single cells were isolated from spleen, lymph node, and peripheral blood using standard protocol. All isolated cells were depleted of erythrocytes by hypotonic lysis. For CyTOF analysis, cells were blocked for Fc γ R using CD16/CD32 antibody (clone 2.4G2, BD Biosciences) and incubated with CyTOF antibody (DVS Sciences, used at 0.5 test/1 million cells) for 30 minutes at room temperature. Cells were washed once and incubated with MAXPARNucleic Acid Intercalator-¹⁰³Rh (DVS Sciences) for 20 minutes for viability staining. Cells were fixed with 1.6% formaldehyde for 1 hour and incubated with MAXPARNucleic Acid Intercalator-Ir (DVS Sciences) at 4°C overnight to stain the nuclei. The samples were analyzed with CyTOF instrument (DVS Sciences) in the Flow Cytometry and Cellular Imaging Core Facility at the MD Anderson Cancer Center. Flow cytometry was performed using standard protocol on LSRFortessa analyzer (Becton Dickinson) and analyzed with FlowJo software (Tree Star).

T-cell Suppression and MDSC Migration Assay

T-cell suppression assay was performed as described (9) using FACS-sorted MDSCs and CFSE (Invitrogen)-labeled MACS-sorted (Miltenyi Biotec) CD8⁺ or CD4⁺ T cells in anti-CD3- and anti-CD28-coated 96-well plates at an MDSC/T-cell ratio of 0:1, 1:1, 1:2, 1:4, with 3.0×10^5 to 5.0×10^5 MDSCs used in each ratio. Cells were analyzed after 72 hours by flow cytometry, and the suppression of T cells is calculated as described (41). The percentage of CFSE⁺ cells divided in the presence of MDSCs was compared with the percentage of CFSE⁺ divided cells in the absence of any added MDSCs. For the MDSC migration assay, an equal number of FACS-sorted MDSCs, untreated or pretreated with neutralizing antibody or inhibitor, were placed on the upper chamber of a transwell system (BD Falcon), and conditioned media from PTEN/SMAD4-deficient cells under various conditions were added to the bottom chamber. Cells were allowed to migrate to the bottom well for 6 hours at 37°C with 5% CO₂. Migrated cells were then analyzed by flow cytometry using BD Fortessa X20. Migrated FITC-positive cells were gated to count the absolute number of cells migrated through the transwell.

MDSC Depletion In Vivo with Gr1 Antibody, Peptibody, and CXCR2 Inhibitor SB225002

Anti-Gr1 (clone RB6-8C5) and isotype control (clone LTF2) were purchased from BioXcell and dosed at 200 μ g/mouse (i.p.) every other day. Endotoxin-free plasmids (15 μ g) for irrelevant control peptibody (Irr-pep) and MDSC-specific Pep-H6 peptibody were injected into mice through tail vein using the established protocol (21) in TransIT-EE Delivery Solution (Mirus Bio LLC) every 4 days. SB225002 (Cayman Chemical) in DMSO was diluted in vehicle (0.9% NaCl, 0.3% Tween 80) for *in vivo* administration every other day (5 mg/kg).

Inducible Yap1 Knockdown

Inducible *Yap1* knockdown was constructed by cloning the two *Yap1* shRNAs used previously (26) from the pLKO.1 into a doxycycline-inducible plasmid. Lentivirus was packaged in 293T and was used to infect PPS, a C57BL/6-syngeneic cell line isolated from prostate tumor of *Pten*^{pc/-}*Smad4*^{pc/-}*Trp53*^{pc/-} mice. Stable sublines were selected with puromycin (2 μ g/mL) and injected subcutaneously to the flank of 5-week-old male C57BL/6 mice (Jackson Laboratory). Two weeks after injection, mice were fed with doxycycline water (2 g/L), a method used to execute doxycycline-inducible expression *in vivo* (42). Tumors were measured and extracted 6 days later to analyze for MDSC percentage in infiltrating immune cells.

Computational Analysis of Mouse Microarray Data and Human Prostate TCGA Data

RNA was isolated from FACS-sorted GFP⁺ and Tomato⁺ cells using *Pten*^{PC-/-}*Smad4*^{PC-/-}*mTmG*⁺ prostate tumors, followed by microarray analysis at the MD Anderson Microarray Core facility using the Mouse Genome 430 2.0 Array (Affymetrix) to generate a *Pten*^{PC-/-}*Smad4*^{PC-/-} tumor/stroma dataset GSE71319. Dataset GSE25140 was downloaded from the NCBI Gene Expression Omnibus (GEO) database. Differentially expressed genes between two conditions (GFP⁺ vs. Tomato⁺ or PTEN/SMAD4 vs. PTEN) were subjected to IPA, GSEA, and oPOSSUM analysis. For analysis of human prostate data, we first generated a list of 39 human MDSC signature genes by literature mining (Supplementary Table S7). The gene expression data of 498 TCGA prostate samples were downloaded from the Broad GDAC Firehose (<http://gdac.broadinstitute.org>), which is the RSEM expression estimates normalized to set the upper quartile count at 1,000 for gene level and then with log₂ transformation. The 498 TCGA prostate samples were clustered using the 39 MDSC genes into MDSC-high, MDSC-low, and MDSC-medium (distance between pairs of samples was measured by Manhattan distance, and clustering was then performed using complete-linkage hierarchical clustering). Sixty-nine samples from Wallace and colleagues (32) were clustered into MDSC-high and MDSC-low. Differentially expressed genes between MDSC-high and MDSC-low were analyzed by GSEA. The expression of *CXCL6* in MDSC-high samples is compared with MDSC-low samples using the Wilcoxon test.

Immunohistochemistry and Western Blot Analysis

Tissues were fixed in 10% formalin overnight and embedded in paraffin. IHC was performed as described earlier (11). For Western blot analysis, cells were lysed on ice using RIPA buffer (Boston Bio-Products) supplemented with protease and phosphatase inhibitors (Roche). YAP1 antibody was obtained from Novus Bio and Cell Signaling Technology. CXCL5 antibodies were obtained from Bioss and R&D Biosystems. CXCR2 antibody was obtained from Bioss and R&D Biosystems. CD45 and Ly6G antibodies were obtained from Biolegend. Prostate tissue microarray was obtained from Folio Bioscience.

Chromatin Immunoprecipitation

ChIP was performed as described (26) using YAP1 antibody from Novus. Briefly, 5 µg of rabbit IgG (Santa Cruz) or YAP1 antibody was incubated with Protein A Dynabead magnetic beads (Invitrogen) for 4 hours, followed by extensive wash to remove unbound antibody. Antibody beads were then added to the chromatin and incubated overnight. The following primers were used for qPCR analysis: CXCL5_S: 5'-CTCCAGTTTCCTGCCTGAAG-3' and CXCL5_as: 5'-GTGTGGAGATTGGGGCTCTA-3'.

Quantitative RT-PCR

RNA was isolated by the RNeasy Kit (Qiagen) and reverse transcribed using the Superscript III cDNA Synthesis Kit (Life Technology). Quantitative PCR was performed using the SYBR-GreenER Kit (Life Technology). The following primers were used: CXCL5_Fwd: GCATTTCGTGTTGCTGTTACGCTG, CXCL5_Rev: CTCCTTCTGGTTTTTCATGTTTAGC; β-actin_Fwd: GAAATCGTGCGTGACATCAAAG, β-actin_Rev: TGTAGTTTCATGGATGCCACAG; YAP1_Fwd: TGAGATCCCTGATGATGTACCAC, YAP1_Rev: TGTTGTTGTCTGATCGTTGTGAT.

Statistical Analysis

Data are presented as mean ± SD unless indicated otherwise. The Student *t* test assuming two-tailed distributions was used to calculate statistical significance between groups. Animal survival benefit was

determined by the Kaplan–Meier analysis. *P* < 0.05 was considered statistically significant.

Accession Numbers

The expression array data used in this article were in GEO with accession numbers GSE25140 (11) and GSE71319.

Disclosure of Potential Conflicts of Interest

A. Kapoor is a research investigator at Novartis. C.J. Logothetis has received commercial research grants from Astellas, BMS, J&J, Excelsis, Pfizer, Novartis, Bayer, AstraZeneca, and Helsinn HC. No potential conflicts of interest were disclosed by the other authors.

Authors' Contributions

Conception and design: G. Wang, X. Lu, Z. Ding, C.J. Logothetis, Y.A. Wang, R.A. DePinho

Development of methodology: G. Wang, X. Lu, P. Dey, P. Deng, V. Ramamoorthy, Q. Chang

Acquisition of data (provided animals, acquired and managed patients, provided facilities, etc.): G. Wang, X. Lu, P. Dey, P. Deng, Z. Fang, S. Hua, E.M. Li-Ning-Tapia, Z. Guo, X. Shang, S. Khadka, E.-J. Jin, X. Pan, L. Li, Q. Chang, P. Troncoso, M.J. McArthur

Analysis and interpretation of data (e.g., statistical analysis, biostatistics, computational analysis): G. Wang, X. Lu, P. Dey, C.C. Wu, J. Zhang, C.-J. Wu, N.B. Patel, Y. Shi, Q. Chang, C.J. Logothetis, M.J. McArthur, Y.A. Wang

Writing, review, and/or revision of the manuscript: G. Wang, X. Lu, P. Dey, C.C. Wu, C.-J. Wu, C.J. Logothetis, M.J. McArthur, Y.A. Wang, R.A. DePinho

Administrative, technical, or material support (i.e., reporting or organizing data, constructing databases): P. Dey, P. Deng, C.C. Wu, S. Jiang, R. Konaparthi, E.M. Li-Ning-Tapia, A. Kapoor, N.B. Patel, Z. Guo, T. Heffernan, D. Zhao, X. Shang, P. Hou, B. Hu, W. Yao, Y. Shi, L. Chin

Study supervision: Y.A. Wang, R.A. DePinho

Other (mouse work): K. Zhao

Other (assessed immunohistochemical stains): E.M. Li-Ning-Tapia
Other (supported molecular biology needs, i.e., cloning): T.N. Tieu

Acknowledgments

The authors thank Drs. Larry W Kwak and Hong Qin for the peptidyl plasmids; Drs. Willem Overwijk and Yared Hailemichael for advice in hydrodynamic injection; Samirkumar Amin and members of the DePinho laboratory for helpful suggestions and technical support; and the Flow Cytometry and Cellular Imaging Core Facility (Jared Burks, Duncan Mak, and Karen Dwyer) and the Sequencing & Non-coding RNA Core Services (Chang-Gong Liu) at The University of Texas MD Anderson Cancer Center (Cancer Center Support Grant CA16672).

Grant Support

The project was supported by U01CA141508 (to L. Chin and R.A. DePinho), Prostate Cancer Research Program (PCRP) W81XWH-13-1-0202 (to G. Wang) and W81XWH-14-1-0429 (to P. Dey); the Idea Development Award–New Investigator Option (W81XWH-14-1-0576; to X. Lu) from the Department of Defense; and the Clayton & Modesta Williams Cancer Research Fund. Additional support was provided by the Jane Coffin Childs Memorial Fund Postdoctoral Fellowship to X. Lu. E.-J. Jin is supported by Korean Governments (MISP) grant number 2011-0030130.

Received February 23, 2015; revised October 5, 2015; accepted October 16, 2015; published OnlineFirst December 23, 2015.

REFERENCES

- Karlou M, Tzelepi V, Efstathiou E. Therapeutic targeting of the prostate cancer microenvironment. *Nat Rev Urol* 2010;7:494–509.
- Junttila MR, de Sauvage FJ. Influence of tumour micro-environment heterogeneity on therapeutic response. *Nature* 2013;501:346–54.
- Hanahan D, Coussens L. Accessories to the crime: functions of cells recruited to the tumor microenvironment. *Cancer Cell* 2012;21:309–22.
- Hanahan D, Weinberg Robert A. Hallmarks of cancer: the next generation. *Cell* 2011;144:646–74.
- Talmadge JE, Gabrilovich DI. History of myeloid-derived suppressor cells. *Nat Rev Cancer* 2013;13:739–52.
- Vuk-Pavlović S, Bulur PA, Lin Y, Qin R, Szumlanski CL, Zhao X, et al. Immunosuppressive CD14+HLA-DRlow/- monocytes in prostate cancer. *Prostate* 2010;70:443–55.
- Idorn M, Kollgaard T, Kongsted P, Sengelov L, Thor Straten P. Correlation between frequencies of blood monocytic myeloid-derived suppressor cells, regulatory T cells and negative prognostic markers in patients with castration-resistant metastatic prostate cancer. *Cancer Immunol Immunother* 2014;63:1177–87.
- Brusa D, Simone M, Gontero P, Spadi R, Racca P, Micari J, et al. Circulating immunosuppressive cells of prostate cancer patients before and after radical prostatectomy: profile comparison. *Int J Urol* 2013;20:971–8.
- Garcia AJ, Ruscetti M, Arenzana TL, Tran LM, Bianci-Frias D, Sybert E, et al. Pten null prostate epithelium promotes localized myeloid-derived suppressor cell expansion and immune suppression during tumor initiation and progression. *Mol Cell Biol* 2014;34:2017–28.
- Di Mitri D, Toso A, Chen JJ, Sarti M, Pinton S, Jost TR, et al. Tumour-infiltrating Gr-1+ myeloid cells antagonize senescence in cancer. *Nature* 2014;515:134–7.
- Ding Z, Wu CJ, Chu GC, Xiao Y, Ho D, Zhang J, et al. SMAD4-dependent barrier constrains prostate cancer growth and metastatic progression. *Nature* 2011;470:269–73.
- Bjornson ZB, Nolan GP, Fantl WJ. Single-cell mass cytometry for analysis of immune system functional states. *Curr Opin Immunol* 2013;25:484–94.
- Youn JI, Nagaraj S, Collazo M, Gabrilovich DI. Subsets of myeloid-derived suppressor cells in tumor-bearing mice. *J Immunol* 2008;181:5791–802.
- Kusmartsev S, Nefedova Y, Yoder D, Gabrilovich DI. Antigen-specific inhibition of CD8+ T cell response by immature myeloid cells in cancer is mediated by reactive oxygen species. *J Immunol* 2004;172:989–99.
- Szuster-Ciesielska A, Hryciuk-Umer E, Stepulak A, Kupisz K, Kan-defer-Szerszen M. Reactive oxygen species production by blood neutrophils of patients with laryngeal carcinoma and antioxidative enzyme activity in their blood. *Acta Oncol* 2004;43:252–8.
- Schmielau J, Finn OJ. Activated granulocytes and granulocyte-derived hydrogen peroxide are the underlying mechanism of suppression of T-cell function in advanced cancer patients. *Cancer Res* 2001;61:4756–60.
- Pekarek LA, Starr BA, Toledano AY, Schreiber H. Inhibition of tumor growth by elimination of granulocytes. *J Exp Med* 1995;181:435–40.
- Wang G, Lunardi A, Zhang J, Chen Z, Ala U, Webster KA, et al. Zbtb7a suppresses prostate cancer through repression of a Sox9-dependent pathway for cellular senescence bypass and tumor invasion. *Nat Genet* 2013;45:739–46.
- Lunardi A, Ala U, Epping MT, Salmena L, Clohessy JG, Webster KA, et al. A co-clinical approach identifies mechanisms and potential therapies for androgen deprivation resistance in prostate cancer. *Nat Genet* 2013;45:747–55.
- Qin H, Lerman B, Sakamaki I, Wei G, Cha SC, Rao SS, et al. Generation of a new therapeutic peptide that depletes myeloid-derived suppressor cells in tumor-bearing mice. *Nat Med* 2014;20:676–81.
- Liu F, Song Y, Liu D. Hydrodynamics-based transfection in animals by systemic administration of plasmid DNA. *Gene Ther* 1999;6:1258–66.
- Muzumdar MD, Tasic B, Miyamichi K, Li L, Luo L. A global double-fluorescent Cre reporter mouse. *Genesis* 2007;45:593–605.
- Yang L, Huang J, Ren X, Gorska AE, Chytil A, Aakre M, et al. Abrogation of TGF beta signaling in mammary carcinomas recruits Gr-1+CD11b+ myeloid cells that promote metastasis. *Cancer Cell* 2008;13:23–35.
- Bierie B, Stover DG, Abel TW, Chytil A, Gorska AE, Aakre M, et al. Transforming growth factor-beta regulates mammary carcinoma cell survival and interaction with the adjacent microenvironment. *Cancer Res* 2008;68:1809–19.
- Johnson R, Halder G. The two faces of Hippo: targeting the Hippo pathway for regenerative medicine and cancer treatment. *Nat Rev Drug Discov* 2014;13:63–79.
- Kapoor A, Yao W, Ying H, Hua S, Liewen A, Wang Q, et al. Yap1 activation enables bypass of oncogenic Kras addiction in pancreatic cancer. *Cell* 2014;158:185–97.
- Shao DD, Xue W, Krall EB, Bhutkar A, Piccioni F, Wang X, et al. KRAS and YAP1 converge to regulate EMT and tumor survival. *Cell* 2014;158:171–84.
- Zhao B, Li L, Wang L, Wang CY, Yu J, Guan KL. Cell detachment activates the Hippo pathway via cytoskeleton reorganization to induce anoikis. *Genes Dev* 2012;26:54–68.
- Nguyen LT, Tretiakova MS, Silvis MR, Lucas J, Klezovitch O, Coleman I, et al. ERG activates the YAP1 transcriptional program and induces the development of age-related prostate tumors. *Cancer Cell* 2015;27:797–808.
- Kwon AT, Arenillas DJ, Worsley Hunt R, Wasserman WW. oPOSSUM-3: advanced analysis of regulatory motif over-representation across genes or ChIP-Seq datasets. *G3* 2012;2:987–1002.
- Ding Z, Wu C-J, Jaskelioff M, Ivanova E, Kost-Alimova M, Protopopov A, et al. Telomerase reactivation following telomere dysfunction yields murine prostate tumors with bone metastases. *Cell* 2012;148:896–907.
- Wallace TA, Prueitt RL, Yi M, Howe TM, Gillespie JW, Yfantis HG, et al. Tumor immunobiological differences in prostate cancer between African-American and European-American men. *Cancer Res* 2008;68:927–36.
- Chen Z, Trotman LC, Shaffer D, Lin HK, Dotan ZA, Niki M, et al. Crucial role of p53-dependent cellular senescence in suppression of Pten-deficient tumorigenesis. *Nature* 2005;436:725–30.
- Liu Q, Russell MR, Shahriari K, Jernigan DL, Lioni MI, Garcia FU, et al. Interleukin-1beta promotes skeletal colonization and progression of metastatic prostate cancer cells with neuroendocrine features. *Cancer Res* 2013;73:3297–305.
- Toh B, Wang X, Keeble J, Sim WJ, Khoo K, Wong WC, et al. Mesenchymal transition and dissemination of cancer cells is driven by myeloid-derived suppressor cells infiltrating the primary tumor. *PLoS Biol* 2011;9:e1001162.
- Stromnes IM, Brockenbrough JS, Izeradjene K, Carlson MA, Cuevas C, Simmons RM, et al. Targeted depletion of an MDSC subset unmasks pancreatic ductal adenocarcinoma to adaptive immunity. *Gut* 2014;63:1769–81.
- Gabrilovich DI, Ostrand-Rosenberg S, Bronte V. Coordinated regulation of myeloid cells by tumours. *Nat Rev Immunol* 2012;12:253–68.
- Osanto S, van Poppel H, Burggraaf J. Tasquinimod: a novel drug in advanced prostate cancer. *Future Oncol* 2013;9:1271–81.
- Filipazzi P, Huber V, Rivoltini L. Phenotype, function and clinical implications of myeloid-derived suppressor cells in cancer patients. *Cancer Immunol Immunother* 2012;61:255–63.
- Solito S, Marigo I, Pinton L, Damuzzo V, Mandruzzato S, Bronte V. Myeloid-derived suppressor cell heterogeneity in human cancers. *Ann N Y Acad Sci* 2014;1319:47–65.
- Battaglia M, Stabilini A, Roncarolo MG. Rapamycin selectively expands CD4+CD25+FoxP3+ regulatory T cells. *Blood* 2005;105:4743–8.
- Ying H, Kimmelman AC, Lyssiotis CA, Hua S, Chu GC, Fletcher-Sananikone E, et al. Oncogenic Kras maintains pancreatic tumors through regulation of anabolic glucose metabolism. *Cell* 2012;149:656–70.

CANCER DISCOVERY

Targeting YAP-Dependent MDSC Infiltration Impairs Tumor Progression

Guocan Wang, Xin Lu, Prasenjit Dey, et al.

Cancer Discov 2016;6:80-95. Published OnlineFirst December 23, 2015.

Updated version Access the most recent version of this article at:
doi:[10.1158/2159-8290.CD-15-0224](https://doi.org/10.1158/2159-8290.CD-15-0224)

Supplementary Material Access the most recent supplemental material at:
<http://cancerdiscovery.aacrjournals.org/content/suppl/2015/12/18/2159-8290.CD-15-0224.DC1.html>

Cited articles This article cites 42 articles, 12 of which you can access for free at:
<http://cancerdiscovery.aacrjournals.org/content/6/1/80.full.html#ref-list-1>

E-mail alerts [Sign up to receive free email-alerts](#) related to this article or journal.

Reprints and Subscriptions To order reprints of this article or to subscribe to the journal, contact the AACR Publications Department at pubs@aacr.org.

Permissions To request permission to re-use all or part of this article, contact the AACR Publications Department at permissions@aacr.org.